

Theoretical Engineering and Satellite Comlink of a PTVD-SHAM System

By Philip Baback Alipour ^{1, 2, *, †}

1-Category of Computer Sciences, Laboratory of Systems Technology,
Research, Design & Development,
Elm Tree Farm, Wallingfen Lane, Newport, Brough, HU15 1RF, UK
2- Computer Science & Engineering Departments, University of Hull,
Cottingham Road, Hull Campus, East Yorkshire, HU6 7RX, UK

Abstract — This paper focuses on super helical memory system’s design, ‘Engineering, Architectural and Satellite Communications’ as a theoretical approach of an invention-model to ‘store time-data’ in terms of anticipating the best memory location ever for data/time. The current release entails three concepts: 1- the in-depth theoretical physics engineering of the chip, including its, 2- architectural concept based on very large scale integration (VLSI) methods, and 3- the time-data versus data-time algorithm. The ‘Parallel Time Varying & Data Super-helical Access Memory’ (PTVD-SHAM), possesses a *waterfall effect* in its architecture dealing with the process of potential-difference output-switch into diverse logic and quantum states described as ‘Boolean logic & image-logic’, respectively. Quantum dot computational methods are explained by utilizing coiled carbon nanotubes (CCNTs) and carbon nanotube field effect transistors (CNFETs) in the chip’s architecture. Quantum confinement, categorized quantum well substrate, and **B**-field flux involvements are discussed in theory. Multi-access of coherent sequences of ‘qubit addressing’ in any magnitude, gained as pre-defined, here e.g., the ‘big \mathcal{O} notation’ asymptotically confined into singularity while possessing a magnitude of ∞ for the orientation of array displacement. Gaussian curvature of $k < 0$ versus $k' > (k < 0)$ is debated in aim of specifying the 2D electron gas characteristics, data storage system for defining short and long time cycles for different CCNT diameters where space-time continuum is folded by chance for the particle. Precise pre/post-data timing for, e.g., seismic waves before earthquake mantle-reach event occurrence, including time varying self-clocking devices in diverse geographic locations for radar systems is given in the corresponding Subsections of the paper. This application could also be optional for data depository versus extraction in the best supercomputer system’s locations, autonomously. The theoretical fabrication process, electromigration between chip’s components is discussed as well.

Keywords: image logic; depository vector; special relativity; carbon nanotube field effect transistor; two-dimensional electron gas; time-data

* Author for correspondence (philipbaback_orbsix@msn.com).

† In-depth architectural science and theory to this topic is submitted to ArXiv.org, ‘Logic, Design and Organization of Parallel Time Varying Data and Time Super-helical Memory; PTVD-SHAM’, Article-id. [arXiv:0707.1151](https://arxiv.org/abs/0707.1151) on 9 Jul 2007. Nevertheless, the current release entails aspects of engineering and theoretical physics including design outcome and algorithmic paradigms, which are not in revision to the original context of the architectural concept.

1 In-depth classical introduction to the physical engineering and architectural concepts

An in-depth classical introduction in retrospect to the basics of electronics and the principles of integrated circuits, is required to give the reader a combination of those basics with a newcomer concept of a system which could be capable of storing data inclusive to time. This so-called ‘data and time’s point of inclusion’ is gradually explained from a general viewpoint in §5 and §§2.2, §§2.3 of §2; from a kinematical-dynamical viewpoint in detail, discussed in the current Section and §4. There is a grave difference in distinguishing the notion of storing data bounded with time, as the data’s obstacle for every memory system and the notion of freedom of choice for data bounded with time, as the data’s barrier break for a parallel time varying data super-helical memory (PTVD-SHAM) system. In fact, this sort of data barrier break, explicates data being bounded with time-independent situations i.e. time-data, where time itself could be stored as a new type of data representing free data displacement (time-independent transmission) in a favorable point of loci. Connote that, the notion of ‘data-time’ must not be confused with ‘time-data’ due to the former merely representing events related to data interdependent with time, where its displacement, i.e. ‘data displacement’, is in a controlled point of assigned loci coming from a programming environment (‘control’ in Eq. 1c). In other words,

$$\text{data} \circ \text{time} \neq \text{time} \circ \text{data}$$

$$\therefore \left\{ \text{data} \circ \text{time} \equiv \frac{\text{data}}{\text{time}} \rightarrow \frac{n \text{ bit}}{\text{s}} \right\} \wedge \left\{ \text{time} \circ \text{data} \equiv \frac{\text{time}}{\text{data}} \rightarrow \frac{k \text{ s}}{\text{bit}} \right\}, \quad n \in \mathbb{N}, \quad k \in \mathbb{Z},$$

$$\therefore \text{data} \circ \text{time} \circ \text{data} = \left\{ f \left(\frac{\text{data.time}}{\text{time.data}} \right) \left| \left[\frac{\text{data}}{\text{time}} \asymp \frac{\text{time}}{\text{data}} \right] \in \mathcal{D} \right. \right\} \rightarrow \mathcal{R}; \text{ equivalently,}$$

$$f : \mathcal{D} \rightarrow \mathcal{R}; \left(\frac{\text{data}}{\text{time}} \asymp \frac{\text{time}}{\text{data}} \right) \mapsto \frac{n \text{ bit}}{\text{qbit s}}, \frac{k \text{ s}}{\text{qbit qs}} \in \{ n \text{ bit} \cap (\text{qbit.s})^{-1}, k \text{ s} \cap (\text{s.qbit})^{-1} \}$$

$$\Leftrightarrow \{ \text{postbit.frequency}, \text{time.prebit} \} \Leftrightarrow \{ \text{data.time}, \text{time.data} \} \quad (1a)$$

thus,

$$\therefore \forall \text{data} \circ \text{time} \neq \forall \text{time} \circ \text{data}. \quad (1b)$$

Let on the one hand, notation \circ for data-time, represent cyclical dependency from data to time and therefore once again to data, denoting ‘data’ in this scenario to be time-dependent under circumstances. On the other hand, the same notation (unless indicated with a ‘ \circ ’) for time-data, represents cyclical dependency from time to data and therefore to data, denoting data to be time-independent allowing time to be storable as well under circumstances. Symbol \asymp , defines an asymptotic relationship between data and time under variant circumstances where ‘data’ is ‘dependant’ otherwise, independent of time and vice versa. Where $k \text{ s}(\text{bit})^{-1}$, does imply to the notion of video cameras and CCDs. That is, capturing images defined as capture rate, k seconds per image, such that in this case, time acts independent in defining the pixel’s locus in an xy -pixel plane for a perfect up to date time-independent graphical resolution. Hence, the second side of the equation in (1a), is defined as image logic as specified in the deduction emerged from it, (1b), whilst on the first side of that equation, is just ‘data per second’ in ordinary computational methods of pure logic rather than

image logic. Ergo, the ‘ \neq ’ use in (1b), stands relevant between equation components, data \circ time, and time \circ data, such that, the *commutative law* for any function composition results a noncommutative condition. Thus, considering a mapping from the asymptotic relationship between time and data regardless of their non-commutativity to bit.frequency (later known as ‘bit frequency’, ν_{bit} , in relation 1.1, §§1.1), results in a prebit concept which is a ‘pre-computed-bit’ in cases where time is intersected with its quantum type. That is, qs (quantum seconds) in terms of, $ks \cap (s)^{-1}$ from $ks \cap (s.qbit)^{-1}$. in the previously stated ‘time data’ relations, one must not confuse point combinator ‘.’, with e.g., dot product and multiplication operators. However, it may be strongly related to fixed point combinator functions in programming.

Most imperatively, in (1.a), the qbit as qubit or quantum bit, is too intersected with its classical binary type i.e. Boolean logic bit. All the previous notions on qs, qbit and logic bit in the content of data \circ time \circ data’s function, appreciate the laws of quantum logic [27, xxiii] whilst possessing image logic and other logical conditions in release. Symbol \mathcal{D} , represents domain, and \mathcal{R} , stands for range. Once the mathematical domain \mathcal{D} , comes justified in terms of function f , the mapping could therefore stand robust in performance on data-time versus time-data for all progressing computations (the use of universal quantifier, \forall , instead of existential quantifier, \exists , in 1.b). This occurs when all intersections of \cap s, against unions of \cup s, vindicated in operators \times , \div , between qbit, qs, against bit and s, respectively.

Furthermore, we already know the notion of ‘algorithm’ by Kowalski [51] in concurrent logic programming is expressed by the equation

$$\text{Algorithm} = \text{logic} + \text{control}, \quad (1c)$$

where ‘logic’ represents a logic program and ‘Control’ represents different theorem-proving strategies [27, .xvii]. Wherein contrast, the definition of ‘algorithm’ in computer science, for cases of PTVD-SHAM algorithms, could be expressed as

$$\text{PTVDA} \hat{=} \text{Parallel Time Varying Data Algorithm},$$

whereby,

$$\begin{aligned} \text{PTVDA} &= \text{image logic} + \text{logic} + \text{freed control} \\ &= \text{image logic} + \text{logic} + \text{automated control}. \end{aligned} \quad (1d)$$

Let notation, $\hat{=}$, represent ‘stands for...’ [12] in models of specification logic. Ergo, in Eq. (1.c), logic $\hat{=}$ logic program; in Eq. (1.d), image logic $\hat{=}$ image logic program combining one or more than one logic and image state into one data collection (see §3, §4, and explanations provided on Figs. 1.1, 1.2); freed control or automated control or auto-control $\hat{=}$ different theorem-proving in a freed favourable state e.g., in favour of data and its address (data addressing). This type of data-addressing shan’t jeopardize the approach of say, a computer programmer’s coding and addressing bits of information between the elements of an array. However, it is the data itself in this ‘PTVD algorithm’ acting time-independent in a loop of storable time frames, refreshing all data types iteratively. This data iteration (tail-recursion) for n elements divided into p sublists for the PTVDA’s p processors in the PTVD-SHAM system, occurs whilst any external sorting algorithm in memory sorts elements randomly in parallel or,

$$\mathcal{O}\left(\frac{n}{p} \log\left(\frac{n}{p}\right)\right) \rightarrow f(n)_{\text{PTVD}} = \mathcal{O}(n) \wedge T(n)_{\text{PTVD}} | T(n) \in \mathcal{O}(n^2)$$

where,

$$T(n)_{\text{PTVD}} = \mathcal{O}(n \log(n)) : \mathcal{O}(n' \log(n)), \{n' \leftrightarrow n\} \circ \{M \vee \infty\} | n' \parallel n, M \in \mathbb{R}^+$$

(1e)

subsequently, assuming for $\{n' \leftrightarrow n\}$, this

$$\forall n, n' \in T(n)_{\text{PTVD}}, \exists \frac{n}{n'} = 1 \Leftrightarrow \{n' = n\} \bigvee \frac{n'}{\infty} \Leftrightarrow \{n \rightarrow \infty\} \bigvee \frac{\infty}{M} \Leftrightarrow \{n' \rightarrow M\}, \quad (1f)$$

thence, in approximation to a mathematical function on PTVDA, and benefiting from idempotence law in Boolean algebra on $\mathcal{O}(n)$ of (1e), one could henceforth write

$$\begin{aligned} \therefore f(n)_{\text{PTVD}} = \mathcal{O}(n) : \mathcal{O}(n') &= \left\{ \begin{array}{l} 0 \bigvee \infty \bigvee 1 \circlearrowleft \mathcal{O}(n) \\ \mathcal{O}(n') \circlearrowright 1 \bigvee \infty \bigvee 0 \end{array} \right\} \\ &= \mathcal{O}(n') \circlearrowright \{0, 1, \infty\} \circlearrowleft \mathcal{O}(n) \end{aligned} \quad (1g)$$

where original data yet remains to be preserved as it was in form and time complexity. In reality, the ‘original data’ is being displaced across array elements satisfying the best optimized processing system interconnected to the chip e.g., a central processing unit (CPU). Symbol \mathcal{O} in (1e), represents the ‘big O notation’ and the adaptation of this relation is described in the context of ‘parallel sorting algorithms’ [56] defining the sorting and space complexity. Restriction, $|n' \parallel n$, denotes to ‘infinite asymptotics’ [27, xxii], whereon the PTVDA, the n^2 time complexity is conquered by prime elements or parallel elements of n as, n' , thus to maintain eventually cyclical dependencies in relations of (1.a) due to the deduced ratio, $\mathcal{O}(n) : \mathcal{O}(n')$, in the context of simultaneous continuum of time-data/data-time sorting between PTVD-SHAM poles, α and β (specified in the coming Subsection and §2). These dependencies corroborate with the notion made earlier on data-time in (1a). Symbol M , represents a positive real number satisfying an iff condition (denoted by a, ‘ \Leftrightarrow ’) for the estimated size on n parallel to n' . We basically assumed definitive divisions between n and n' in Pred. (1.f), where it could be suppositional in an opposite manner, and in all scenarios of computational complexity theory, they should maintain near 1, 0 or near ∞ via set, $\{0, 1, \infty\}$. Note that, \circlearrowleft and \circlearrowright in (1g), reciprocally define a directional dependency to ∞ but not absolute ∞ . This dependency too, applies for 1 and 0 in the given set (compare with Ref. [27, xxii]). Therefore, equation (1g), would back up the definition, ‘automated control’, for a successful or stable PTVDA in operation, given in (1d).

In the following discussions, we henceforth debate on a system that fundamentally revolutionizes basic semiconductors’ layout design and organization. The current invention-model also inducts an infrastructure which leads the chip to store data quite effectively and efficiently, no matter the definition of traditional data type, data sorting and array dispositions (here, data controllability and management). To this account, one elementary fact remains and that is: ‘computation requires a matrix model to compute values of input information categorically, hence giving an output evaluating the accuracy of the constructed matrix model... if not, the design would be said to have had a major flaw’. Nonetheless, array composition is of the main operative state and an engineer’s interest, resulting appropriate models to arithmetic logic unit (ALU) standards. This model, is to be developed into parallel arithmetic logic unit (PALU) continuum, which performs new independent storable signals of qubit and classical bits of information in one electronics package.

As a result, data would have a freedom of choice to choose ‘where to actually be stored at’, without worrying about its future and previous state of memory address. The user though, accesses data in a virtual state who normally expects from his/her

operating system (e.g. Windows XP-OS) environment. Even problems such as data defragmentation, spending time on heavy amount of lines of coding and compilation issues are resolved dramatically by this design, in practice.

In this Section, we shall explain the energy state and product of sequences of data in a state of conservation of data events across the depository layers of PTVD-SHAM. The PTVD-SHAM is in relevance to §2 in terms of its incorporation of electrical property, addition to optoelectrical property as an extension to the initial construction of PTVD-SHAM. It is also deduced and thus hypothesized that, mathematical formalism of proper time $\Delta\tau$ in some temporal coordinate against relativistic time Δt , in Einstein's special theory of relativity (SR), could be stored for precise self-timing of parallel and non-parallel I/O streams of data in a controlled manner. Concerning these types of I/O data-streams, no matter the complexity of time dilation problem [27, xvi], asynchronous data versus synchronous data, are to be built into one state of time-data state as a compact reliable precision point of time and data in this process.

1.1 Principles and introduction

Possessing the fact that multiple qubits can exhibit quantum entanglement (see, e.g., qubit entanglement [27, xv]), a solution to store the entangled Bell states of electrons from 2DEG system, moving free into the two-dimensional plane, now to some complex plane's depository vector system defining storable qubit(s), is thus emerged in practice.

Furthermore, binary values by binary variable, bit_i as input signal $\forall A_{in} \in \{0, 1\}$ by ratio to qubit variable as input signal B_{in} , are introduced via bit-frequency

$$\nu_{bit} \equiv \frac{A_{in}}{B_{in}t} \left| \text{for } A_{in} \left\{ \begin{array}{l} 0 \triangleq L_{\pm V} \\ 1 \triangleq H_{\pm V} \end{array} \right\} \text{for } B_{in} : |\Psi\rangle = \prod_{m=1}^n |\Psi\rangle_m, m = 1, 2, \dots, n, \quad (1.1)$$

which is in the memory system's product, hereby of importance to generate quantum efficiency for hot-electron spectra. With response to mathematical relations in defining the characteristics of the storage layers of the memory system (subsequent relation), relation (1.1), distributes into future relations (5.1) to (5.5), §5, explaining events related to low-voltage differential signaling (LVDS) e.g., [38]. Specifically, these voltages are computed between components of the memory's staircase levels in terms of V_{in} , addition to stored charges possessing a quantized voltage $\geq k$ mV amongst memory traps for B_{in} defined from wavefunction $|\psi\rangle$'s Bell states.

In possession of the previous relation, simplifying Bell states' relations concerning collectable data points as quantum dots embedded in a 2DEG layer of the high electron mobility transistor (HEMT; for higher state of carrier's mobility) and metal-oxide semiconductor field-effect transistor (MOSFET technology), did not require the study of spin conditions. The requirement to examine the four well-known Bell states' scenarios during the course of entanglement in the 3D space where CNT coils remain, was also eliminated. In fact, from the point of particle confinement, a depository vector emergence by some arbitrary angle for a storable qubit in the storage film, to the point of storing Boolean and qubit data as the lower layers of the semiconductor's gate electrode, is studied theoretically. In addition, the present chip design's architecture appreciates Choi *et al.* of [6]'s 'MOSFET technology utilizing CNTs', to some extent in application's design basics thus not entirely covering the final design outlook itself.

The latter and former paragraphs are preferred as the main objective of the fabrication process rather than studying the probabilistic nature of entangled N-tuplets between the remaining gates in a staircase manner. That is, *quantum confinement*

against entanglement Fermi-level regime, where the Fermi energy is ought to be determined where the electron concentration and effective mass [27, x] meet.

In this case, it is imperative to assess the mass confined into the depository's vector bands of the memory for an observable quantum efficiency quantity within the memory cell's domain (e.g., compare with [5]). In contrast, here, 'quantum efficiency' is not of 'the number of collected electrons over the number of incident photons' for a solar cell defining its level of responsivity via factor of absorption coefficient. In fact, this quantity is studied by the perception that supports resonant cavity layers to the actual memory cell layers of the chip in terms of

$$\begin{aligned} \eta_{\mathfrak{f}} &= \frac{\text{output}_{\mathfrak{f}}}{\text{input}_{\mathfrak{f}}} = \frac{\text{number of electrons collected}}{\text{storable number of ballistic hot electrons in entanglement}} \\ &= \frac{N_e}{N_{e \xrightarrow{L_V, H_V} |\Psi\rangle}}. \end{aligned} \quad (1.2)$$

This relation is of fermion type; both quanta input and output paradoxically are of fermions. Thus, the term 'fermionic quantum efficiency' stands pertinent for hot electrons or hot carriers denoting the principle behaviour of quasi-Fermi characteristics upon the incoming hot electrons from 2DEG staircase layers in entanglement.

The latter carrier characteristics is due to the grouping result of poles: α , β in Fig. 2.1, §2. This effect comes from CCNTs that subjugate mobile carriers to act directional in favour of the entangled wavevector approaching storage cells for all incoming electrons from the 2DEG system to 3D-space, subsequently, committed to a 2D-quantum capacitor of the memory cell. The entangled wavevector is hence derived via, $\mathfrak{E} \equiv (e\sqrt{-1e_2e_2'}) \hat{i}$, elicited from relations (4.1) to (4.11), §4, in satisfaction of the context of Hyp.4.1. In continue,

$$\prod E_{e \xrightarrow{L_V, H_V} |\Psi\rangle} = \frac{1}{nE_{|\Psi\rangle}} \int_d F_e \cdot dd_{xy,z} = \frac{E_{e,z} \times E_{\mathfrak{E}} + E_{e,xy} \times E_{\mathfrak{E}}}{E_{|\Psi\rangle}}, \text{ and}, \quad (1.3)$$

$$\therefore E_{e,xy} \xrightarrow{E_{|\Psi\rangle}} \forall E_{\mathfrak{E}} \in k_C Q \sqrt{QQ'} (2\sqrt{xy} \circ A_{x_i y_i})^{-1} \Big| k_C = \frac{1}{4\pi\epsilon_0} \approx 8.988 \times 10^9 \text{Nm}^2\text{C}^{-2},$$

thus,

$$\begin{aligned} &= \left(k_C |\mathfrak{E}| \left\{ \frac{\hbar^2 k_x^2}{2m_e} + \frac{\hbar^2 k_y^2}{2m_e} + \frac{\hbar^2 k_z^2}{2m_e} \right\} \right)^{\frac{1}{2}} = \sqrt{\frac{k_C |\mathfrak{E}| \hbar^2}{4d_{xy,z} m_e}} = \sqrt{\frac{k_C |\mathfrak{E}| \hbar^2}{4V_{xyz} m_e}} \geq 0 \text{ J} \\ &, |\mathfrak{E}|^2 \equiv e^2 e_1 e_2 \hat{i}^2, k = (k_x, k_y, k_z), d \equiv x \circ \mathbf{k}, y \circ \mathbf{k}, z \circ \mathbf{k}, \end{aligned} \quad (1.4)$$

where $E_{|\Psi\rangle}$, represents the probable energy expectation on wavefunction, $|\psi\rangle$'s Bell states product from (1.1), for the amount of work done in spatial dimensions d_{xy} satisfying $E_{\mathfrak{E}}$ as the energy of the entangled wavevector, \mathfrak{E} . Dimension d_z in return, satisfies $E_{e,z}$ as the energy of the 2DEG or in general, the energy of D-dimensional, $g(E_e) \sim E_e^{(D-2)2^{-1}}$, from the point of quantum wells to the point of charge's storage trap(s), correspondingly. In addition, \mathbf{k} for energy $E_{e,z}$, is in regard to Leadley of [22]'s wavevector definition used to describe a free particle of mass m when it's in confinement, however, not being in entanglement, e.g., the choice of z -direction in the 2D system. Entangled energy $E_{\mathfrak{E}}$, in the energy product is of scalar form, thus the magnitude of energy is of interest and not its direction, since the direction is already

exhibited by directions of $E_{|\Psi\rangle}$ in the denominator's distribution area via implication, $E_{e,xy} \xrightarrow{E_{|\Psi\rangle}} E_e$. In other words, the more energy distribution of E_e in favour of direction z against xy , the more discrete the energy product and thus, partitioned internally. Now, having from relation (2.2) in [10],

$$H_C\psi = E_C\psi, \quad (1.5)$$

and (5.13) from [10], whilst benefiting from the current report's relations (1.3) to (1.5), thence,

$$\therefore E_C\psi = \frac{EE_e}{\prod E_{e \xrightarrow{L_V, H_V} |\Psi\rangle}} \prod_{i=1}^n \phi_i, \quad i = 1, 2, \dots, n. \quad (1.6)$$

Let E_e , serve the classical energy expectation on electrons representing circuit component's classical Boolean logic E , which is the non-local energy expectation from the circuit. This non-local energy expectation must be the remaining energy across the circuit sever from E_e and $E_{e \xrightarrow{L_V, H_V} |\Psi\rangle}$, but not the 'local energy' which is the energy associated with the regions outside of the sub-system and thus their interactions with the sub-system (see relation 5.15 from the concept of local energy density in [10]).

By means of which, the levels of degeneracy principle of energy-states from mobile carriers including their probable superposition to storable time and data space locations are discussed by definition. This definition should be relevant to the nature of circuit's capacitance, i.e., degeneration of eignstates corresponding to identical eignvalues of the Hamiltonian in aim of maintaining a symmetry between 'electric potential energy states' (observe relation 1.6) and 'electric flux density'. The degeneracy behaviour in principle, appears from Maxwell's equations in this case, is by clarifying bit frequency ν_{bit} 's physical property and characteristics. Symbol ϕ_i , is one-electron wavefunctions and k_C , in singled-one-electron product of (1.4), is the electrostatic constant from Coulomb's law, whereas without the consideration of e_1e_2t 's relative existence, the remaining component k_Ced^{-1} , is therefore measured in volts.

Perceivably, the atomic units, m_e , \hbar and e for the electronic circuit at time $t = 0$ represent a closed loop of Hamiltonian type denoting the time evolution of quantum states for the entire circuit once the current flows, hence computing the total energy of the system. It is also perceived that in this case, all corresponding equations are of ratio time-dependent Schrödinger's equation (not time-dependent) via time factor \hat{t} of \mathfrak{E} . This type of equation is governed to be conserved for sufficient capacity, consequently maintaining a time-independent Schrödinger equation expressing a steady-state similar to the indication made on 'quantum sub-systems as circuit blocks', discussed by Delaney & Greer in [10]. Once the shift of pure state at time $t \geq 0$ occurs at some closed-loop state of eignvalues via depository vectors on the memory components, here, the waterfall input/output observable operators, the system's performance as the circuit's power supply is deemed to be not in a pure state any longer. This shift from pure state to a new state occurs, once the fuzziness of 2DEG system and CCNTs comes into practice. In such scenarios, the correlation of inputs and outputs for the involved subsystems could be expressed through the expectation values:

$$\langle \hat{i}\hat{o} \rangle \neq \langle \hat{i} \rangle \langle \hat{o} \rangle. \quad (1.7)$$

Expressing that, 'the inputs and outputs are specified in terms of subsystem observables, or operator expectation values, and these quantities must correlate through a

density matrix' [10], wherein this paper, for the ratio-time-dependent state, we merge the concept into

$$\begin{aligned} \langle \hat{i}\hat{o} \rangle &\xrightarrow{\int_{d\tau}} \langle \hat{i}\hat{o} \rangle = \left\{ \langle \hat{i} \rangle t \frac{\langle \hat{o}_i \rangle}{\tau_\Sigma} = \langle \hat{o} \left(\hat{i}(t) \right) \rangle = f(\hat{o}) = \langle \hat{o}\hat{\tau}_0 \rangle, \right. \\ \tau_\Sigma &\equiv \tau_0 = 1(t_1|t_2), 1(t_2|t_1), \\ \therefore \langle \hat{i}\hat{o} \rangle &= \langle \hat{o}\hat{\tau}_0 \rangle \langle \hat{i}\hat{t} \rangle. \end{aligned} \quad (1.8)$$

$$(1.9)$$

Let time t , be empirically dedicated to operator expectation input value \hat{i} , and asymptotically, the stored proper time τ_Σ dedicated to operator expectation output value \hat{o} . By composition, the interdependency with inputs and their storable proper time including stationary time (or, time at rest) is carried out via, $\hat{o}(\hat{i}(t))$, once the time factor integrals are implied to operator expectation values, $\langle \hat{i}\hat{o} \rangle$. Now, by realizing the time dilation principle [25, 41], and Einstein's relativity [14], one could herein deduce,

Theorem 1.1. *It is supposed that, storable proper time to be the time given to a particle as its time property on its worldline connecting geometric points of field lines of (4.1) with $e^2 e_1 e_2 \hat{t}^2$ of (4.2), §4. The following possessions indicate the conditions of this theorem:*

- (1) *Let $e^2 e_1 e_2 \hat{t}^2$ possess stationary time t_1 and t_2 of $dt \leftrightarrow \tau$ from (4.3) for its unaccelerated worldline with respect to accelerated worldline performed by the involved particle.*
- (2) *The accelerated worldline in possession (1), could be of Gaussian curvature of $k < 0$ representing for \hat{i} 's data, which is being stored in short intervals versus long intervals when the mobile particle's worldline super-symmetry performs, $k' > (k < 0)$, in the context of space-time simultaneity from special relativity.*
- (3) *In possession, these states of curve in (2), could lead to homogeneity of time quantities $t_1|t_2$ and $t_2|t_1$ despite of their highly symmetric relationships (4.2) and (4.3) by representing time factor paradox, $\hat{t}^2 \neq \hat{i}^2$.*

Proof 1.1. *In essence, commences with (4.2), §4, followed by the subsequent logic, then rationalized by, (4.18) & Hyp. 4.1, thereby concludes with, Hyp. 4.2.*

Let the above-mentioned particle in Theorem 1.1, be a storable electron of charge, e , from special relativity (SR). The stored proper time for the inputted data is thereby emerged for its future time in entanglement via 'time barrier' symmetry ($t_1|t_2$) or ($t_2|t_1$), such that, data displacement from one memory location to another throughout the course of time is plausible via the circuit itself as, 'internal data partitioning'. The so-called 'one memory location' is denoted by a '1' which is multiplied by the time symmetry as a unit defining 'data displacement'.

Clearly, there is neither input/output (I/O) external data-partitioning nor I/O union compositions, whereas the given confined 'quantum timing frame' is prior to data type and bus subsystem's way of allocating and program compilation process. This time frame condition is discussed broadly in §4. The chip's dependence upon the I/Os, this time frame establishment therefore encloses operator expectation values, $\langle \hat{i}\hat{o} \rangle$ and $\langle \hat{i} \rangle \langle \hat{o} \rangle$ into a 'satisfied correlated I/O expectation value', $\langle \hat{i}\hat{t} \rangle$ and $\langle \hat{o}\hat{\tau}_0 \rangle$, respectively. These 'correlated I/O expectation values' are for those interconnected

gates with multiple inputs switching simultaneously, which is due to the time and data loop's characteristics, consistent to the following argument's paradox:

————— Contradictorily, as we confront in §4, 'time' for these subsystems behaves in accordance with Russell's Paradox, just as generalized in the calculation made on (1.8) and (1.9). So, the partitioning of a system from a quantum mechanical viewpoint is a resolved point, since the time problem itself is storable in addition to 'read and write data input' process. Hence, perpetuating the steady-state in a loop of subsystems' inputs in correlation to outputs as 'readable data' is proceeded, no matter the degree of freedom defining the role of density matrices, the data in-and-out process is partitioned periodically. That is, partitioning and storing proper time according to future closure relation, (4.14b), §4, specifying, $\tau_\Sigma \approx 0.7071 |\dot{t}_0|$ whilst time, t , is ticking as $t \geq 0$ for the next data write time phase, $WR.\phi_1$, and read time phase, $RD.\phi_1$, operation. —————

Recalling (1.4), we have used the Pythagoras theorem reasoning that, $E_{|\Psi\rangle}$, as hypotenuse according to the initial theorem and, d , later known as radial time distance r , from (4.15), §4. This is the distance recalled for the geometry of revolution in favour of 'depository vector', Σ , in the context of Hyp.4.1. Thus, the entangled wavevector \mathfrak{E} in all product relationships, should also possess a complex number value representing a complex plane in the space and path of electron's transportation. Therefore, this type of quantum efficiency describing products of (1.2) through (1.4), fulfils 'Image Logic' of the storing data, where the necessity of installing catalysts and absorbers across the chip is considered to be vital during chip's fabrication.

In practice, since computer memories require a capacitor that preserves stored charges and a transistor serving as a switch in aim of write data or read data from the capacitor, possessing high transconductance is a must, where FETs in this case, HEMT (e.g., [26]) and MOSFETs are deemed to be the most appropriate technology for this design. To this account, the 'waterfall staircase system' (Fig. 2.1, §2), possesses the switching ability in its fundamental structure. All electrodes in the circuit plan must satisfy write time phase $WR.\phi_1$, and read time phase $RD.\phi_1$, when relevant p.d.'s (potential difference occurrences) are applied between the chip itself and thus its components here as:

————— At least, two CNFET inverters with unequal electrode length L and equal width W by ratio, $L : W$, indicating circuitry's electrical resistance, next to the chip's α -pole; β -pole at δ -pole in the middle. These inverters are connected to a pass transistor logic (PTL) via e.g., a CNFET transmission gate representing time phase ϕ_2 , to refresh all 'symmetric and asymmetric stored data' including, 'asynchronous or non-coordinated time (early, past and future)/'synchronous stored time' and 'data storing event', across the waterfall system into memory cell for either pole (see relations 1.10, 1.11 and Fig. 2.1 of §2)! For this post-mentioned logic, 'time storage, time phase ϕ_2 -values as rise-decay of time phase', is in aim of verifying the process of refreshing time cycles on the α -pole, β -pole and δ -pole data feedback. This is done by PTL layout adjacent to the δ -pole, which is also completed with circuitry's substrate growth and construction phase. —————

Reasonably, the nanodots in the porous film (Fig. 2.1c, §2) in polarity, are positioned below the memory cell's insulating film layer in contact with the CNT. These nanodots are filled with a charge storage material which is one of silicon (Si) and silicon nitride (Si_3N_4) claimed by Choi *et al.* in [6], thus storing charges for a long period of time,

which still requires the determination of ϕ_2 problem in electrical functions. This requirement is due to prioritizing the charges' autonomous repositioning of their space and time occupation across the waterfall system's components (discussed in §4 & §5).

In general, the porous film is made of aluminium oxide (Al_2O_3). The CNT mentioned, is not of a pillar type CNT, and is of semiconducting type, where pillar-CNT by comparison should possess an ohmic electronic behaviour as metallic type unaffected by a gate voltage due to the role of CCNT adjacent to it. With compliance to time phase problems from VLSI basics by Pucknell & Eshraghian of [30], the time phase ratios involved in the poles distributed across the waterfall gate ohmic contacts for 'ideal conditions', is given by

$$\begin{aligned} \langle f(\phi_1)_{(\alpha,\beta,\delta)} \rangle &= \alpha \frac{1}{n} \sum_{i=1}^n (WR.\phi_1 : RD.\phi_1)_i : \beta \frac{1}{n} \sum_{j=1}^n (WR.\phi_1 : RD.\phi_1)_j \\ &= \delta \frac{1}{2} \sum_{k=1}^2 (WR.\phi_1 : RD.\phi_1)_k \end{aligned} \quad (1.10)$$

whereby $n \geq 4$, and the dimensions of the transistors, grouping for these poles explaining sheet resistance, R_s , and measuring resistance, R , of thin films with uniform sheet thickness, θ , including resistivity ρ , shall be,

$$\{\forall L, W \in A \mid Z = L \cdot W^{-1}, R = Z \cdot R_s^{-1}, R_s = \rho\theta^{-1}\}, \{\forall \square \in A \mid L = W, R = R_s\},$$

such that

$$\begin{aligned} \alpha, \beta, \delta. \sum_{k=1}^2 (WR.\phi_1 : RD.\phi_1)_k \neq \delta.\phi_2, \quad \alpha, \beta, \delta. \sum_{k=1}^2 (L : W)_k \neq \alpha'_{90^\circ}. \sum_{l=1}^2 (L : W)_l, \beta'_{90^\circ} \\ \cdot \sum_{m=1}^2 (L : W)_m, \text{ and, } \alpha, \beta, \delta. \sum_{k=1}^2 (L : W)_k \approx \delta'. (L : W). \end{aligned} \quad (1.11)$$

Accordingly, cross-sectional area, A , in the recent predicates could be split into length L and width W describing ratio conditions of Z , henceforth, for any size of square, \square , giving resistance $R = R_s$. Architecturally, notations α , β and δ are just poles with a geometric unit value of '1' in Euclidian space dimensional chip's substrate-occupation, denoted by λ^3 , for the fabricated chip. For circuit layout viewpoints, one could thereby instantiate, $\alpha'_{90^\circ} \cup \beta'_{90^\circ} \parallel \delta'$, where $\delta' \parallel \delta$ and $\delta \not\parallel \delta'$. The complementary pole of δ , is δ' , whereas the latter or former are perpendicular to junctions α'_{90° and β'_{90° , geometrically (Fig. 2.1d, §2).

Associatively, as a preamble to Fig. 2.1, §2, the data flow diagram on p. 11 embeds into its structure, the states of storable time and data in release in form of sequences of bits. This diagram emphasizes on (1.9)'s I/O analog behaviour despite of depository vector's pattern-complexity of inputs/outputs between the chip's logic gates. A loop is generated solely for refreshing time-data cycles via time phase, ϕ_2 . Moreover, this loop, is for storing light purposes which is already apparent to scientists that, storing photons as minute energy packets of electromagnetic radiation into a memory cell is somewhat impossible unless, done in some quantum interference experiment.

It is crucial to not confuse 'time-data' with 'time-varying data' visualized by Joshi & Rheingans in [43], which deals with data in motion and information concerning the kinematics of an arbitrary body in our universe. Even though these people propounded time as individual steps of event counts and snapshots taken for large data-sets (abstract of Ref. [43]), 'time' in the present chip by contrast, denotes to all events of past, current and future, 'simultaneously'. 'Data' however, indicates to all information related to time and space inclusively, once 'time of time-date' is manifested for that particular event's information tuneable to any time location.

So by comparison, on the one hand, ‘data’ itself in this chip is not tuneable autonomously unless dealt with the operating computer user (operator), while on the other hand, ‘time’ is tuneable autonomously in this chip without a human user interaction (operator dependant; HCI dependant).

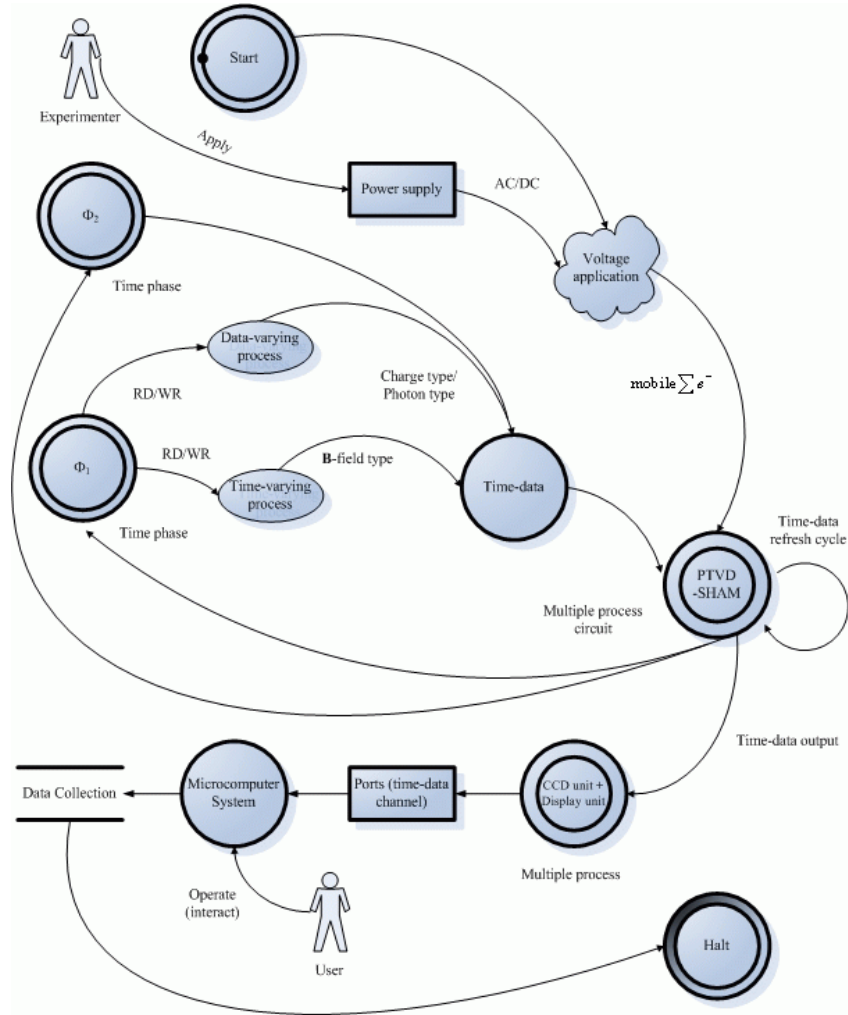


Figure 1.1. A data flow representation of PTVD-SHAM system and I/O behaviour for storing sequences of variant data-time bits on a computer database system. Excited charge, e , and active regions of the α , β , δ poles of the chip are deemed to possess light emitting property via e.g., edge-emitting light emitting diode (ELED). Also, actors of human-computer interaction (HCI) play a vital role in collecting data during PTVD-SHAM’s time-data analysis.

PTVD-SHAM elucidates a new generation of methodologies to store ‘time-data’ parallel to, or, even into light (e.g., [50]), once a few photons are looped between memory’s cavity system and quantum states of photovoltaic effect when the cavity for excited electrons reaches a thermal level above Fermi level (see pp. 14-15). In this

case, the total energy of either form of matter representing bits of information satisfying relation (1.6), could be preserved during data transactions between all memory locations in a cyclical set of: 1- time frame, 2- data frame and 3- converted frame of electrons-light/light-electrons, across the memory channels. These memory channels are of charge material for the non-photonic material (Fig. 2.1c, §2), and optical micro-filters for the path of light installed discretely as an extension to polar sites of α , β or δ (Figs. 1.2; 2.1 of §2). These chip-scale filters govern the intensity, deflections and reflections of a photonic material that carries information whilst being propagated through the system. The photonic material for optical buffering [27, xii], mainly deals with the cavity system, absorbers and filters with a determination factor of light interference and deflection course during operation.

It is conceivable that a chip-scale micro-Faraday filter with apposite direction to an optical fiber plays an important role in-between poles of α and β installed into zone Z' of Fig. 2.1d, §2, isolated from the gate electrodes of either pole in the centre i.e. poles of δ . The optical process of either micro-Faraday filter whilst having their own angle of light deflection, the filters' beam reflection is to preserve interference and coincidence of photons coming from the optical buffer to the receiving unit. The schematic representation of these filters is given in Fig. 1.2, where the method generally maps from the diagrammatic setup of [27, xi] and [49], now into micro chip-scale measurements. Designing the micro-optical fiber complies with light spectra of high/low intensity applications akin to edge-emitting LEDs (ELEDs) layout, does benefit from the following classical equation [46]. The value of the normalized frequency ν , hereinafter referred to as the ν number in an optical fiber path is given by

$$\nu = (2\pi a \lambda^{-1}) \sqrt{n_1^2 - n_2^2}, \quad \sin \theta_1 \sin \theta_2^{-1} = cv^{-1} = n_2 n_1^{-1}, \quad \text{or,} \quad \sin \theta_1 n_1 = \sin \theta_2 n_2. \quad (1.12)$$

where a , is the radius of the fiber core and λ , is the wavelength of the light propagating in vacuo. The ν number of the normalized frequency in (1.12), is a parameter for defining the construction of the optical fiber. In a region in which the ν number is less than 1.57, only a single mode of propagation exists. This region is referred to as: a single mode region. When the ν number increases above 1.57, a greater number of modes appear in proportion to the increase of the ν number [45]. Base upon Snell's law, n_1 and n_2 represent the refractive index of the optical fiber medium, relevant to the principles of optical fiber communications, computing how much the speed of light, v_1 as $c \approx 300000 \text{ kms}^{-1}$, is reduced inside the medium in terms of $c \rightarrow v_2 = v$. Other essential optical measurements in the experimental phase of the PTVD-SHAM project should obey the standards of [46] (see also, §6).

For the chip's time-data in a photon, the design and integration methods of [49], is associated with the current optical buffering system resulting 'Faraday effect', which is based on the classical theory of 'Zeeman effect' as ensued in regard to Hyp. 4.2, §4.

The manifestation procedure, or, Megabit-pixel per second (Mbp s^{-1}) recording system of 'image logic', can be done by incorporating charge-coupled device (CCD)-chipset layer and red-green-blue (RGB) filter, installed above the optical buffer layer. The classical equation is

$$\zeta = \mathcal{V} \mathbf{B} \ell, \quad (1.13)$$

where, magnetic field \mathbf{B} of the equation, is measured in Teslas and is excluded from the \mathbf{B} -field of CCNTs, thus, this field is in enclosure to the magnetic field of the magnets surrounding the vapor cell. Symbol \mathcal{V} , is the Verdet constant for the material measured

in units of radians per Tesla per meter; ℓ , is the length of the path (in meters) where the light and magnetic field interact; ζ , is the angle of rotation measured in radians.

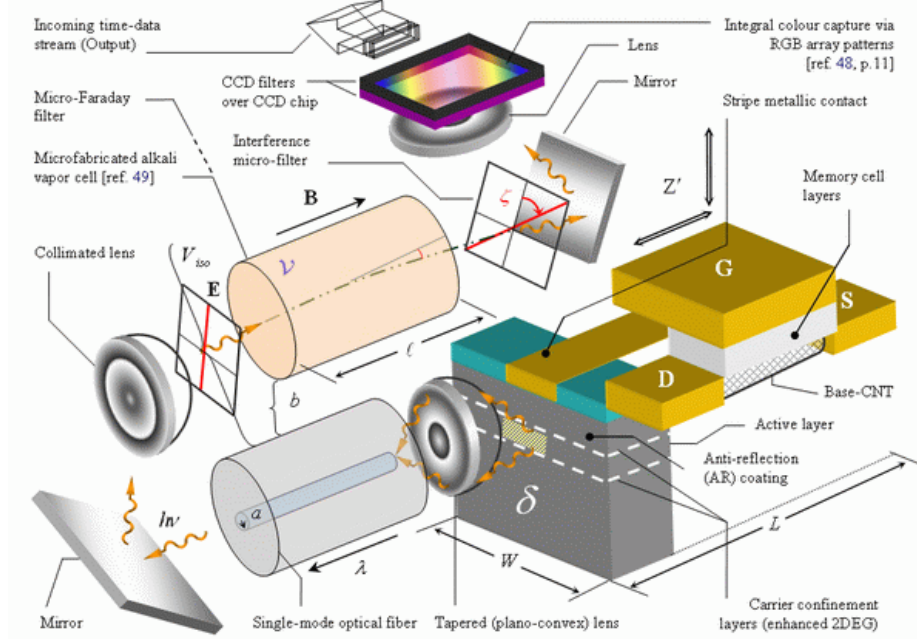


Figure 1.2. A schematic representation of one of the poles, here, the δ -pole, incorporating micro-Faraday filter and optical paths between the active layer of the pole and a CCD. In this design, a plano-convex lens focusing the edge emitting beams of light and a collimated lens, aim to collimate light in parallel lines to the filter. For other chip's poles, if involved, optical coupling and path from source to CCD is required. ELED's light output is of incoherent versus lased-light, based on spontaneous emission versus stimulated emission.

For isolating the magnetic field in the frame of alkali vapor cell with the surrounding magnets from the optical fiber environment, we could also state

$$\begin{aligned}
 \mathbf{A}_{iso} &= \Delta \ell b = 2\pi b(b + \ell) | \mathbf{A}_{iso} \cap \mathbf{B} = 0, \text{ where } \mathbf{V}_{iso} = 2\pi r_C \int_{\min A}^{\max A} f(\mathbf{A}_{iso}) d\mathbf{A}_{iso} = \\
 &= 2\pi \langle r \rangle \ell b, \quad b \ll r_C, \\
 \exists b \wedge \mathbf{B} \rightarrow 0 &= b | b \in \bigwedge_{i=0}^n b_i \ni \\
 \left\{ \begin{array}{l} \text{if } \forall b \wedge \mathbf{B} = \mathbf{B}, \therefore \mathbf{V}_{iso} \not\equiv \mathbf{V}_{iso} \Rightarrow (\mathbf{B}_{iso} : \mathbf{B}) \equiv \frac{\mathbf{B}_{iso}}{\mathbf{B}} = \neg \mathbf{B}_{iso} \in \mathbf{B} \\ \text{if } \forall b \wedge \mathbf{B} \rightarrow 0 = b, \therefore \mathbf{V}_{iso} \equiv \mathbf{V}_{iso} \Rightarrow (\mathbf{B}_{iso} : \mathbf{B}) \equiv \frac{\mathbf{B}_{iso}}{\mathbf{B}} = 1 \end{array} \right\}. \quad (1.14)
 \end{aligned}$$

\mathbf{A}_{iso} , is the slice of isolated surface area (change of rectangular), whereas \mathbf{V}_{iso} , is the isolated cylindrical volume (shell method) from \mathbf{B} -field, expressing the involved magnets for the alkali vapor cell in isolation to the involved optical fiber. Symbol b , denotes the thickness of the shell and, r_C , is the circular radius expressing the involvement of b , being excluded as $b \wedge \mathbf{B} \rightarrow 0 = b$. Otherwise, b , is being included as, $b \wedge \mathbf{B} = \mathbf{B}$, which thereby deduces the volume isolation as not being isolated or, an unsuccessful attempt of \mathbf{B} -field isolation from other circuitry components, paradoxically; i.e. non-isolated \mathbf{B} -field, or, $\neg \mathbf{B}_{iso}$ which is of \mathbf{B} -field type. An 'AND

closure operator', or, $\bigwedge_{i=0}^n b_i$ is here to assist the problem for all limit conditions of b not merely being existential to one b (denoted by symbol \exists , with a commencing zero index identity). Hence satisfying all conditions of b in (1.14), is when b_i intersects with the rest of b -elements for all \mathbf{B} -field isolated/included-ratio, $\mathbf{B}_{iso} : \mathbf{B}$. Similarly, the interference of \mathbf{E} -field with b should also imply to logical conditions of b , as given.

In continue, since $\langle r \rangle$ is the average radius of the shell, the outer radius is, $\langle r \rangle + 2^{-1}b$ and thus the inner radius would be, $\langle r \rangle - 2^{-1}b$. As a result, the volume of the shell is: $(Volume\ of\ micro\text{-}Faraday\ filter) - (Volume\ of\ micro\text{-}vapor\ cell)$, i.e., the deduction made on Pred.(1.14). This theoretical concept of isolating microchip components from one another is believed to be essential, especially when the CCD and lenses are too, associated during and after the fabrication process.

2 Physical-engineering description and principle paradigm of the SHAM chip

Imperatively, with respect to basic circuitry hardware implementation, the engineering aspect of the design relies upon the principles of VLSI in an architectural sense to the PTVD-SHAM chip. Hence, commencing with the theoretical aspect of the general design would guide one to begin with the practical phase, once all values are being thrown at variables, assigning the basic perspective of its simulation results. This phase of the paper merely propounds the theoretical concept of the design, which obeys other people's achievements as referenced to their works with some pending features of the current author. Therefore, summarizing all data events as exemplified in §5, extending the fabrication course of the chip's architecture from §2.1, allows one to test the chip in different environments beyond laboratorial limits.

The following Subsection deals with the major description of the SHAM chip. In §§2.2 and §§2.3, two paradigms are exhibited for the whole design and environmental relationships, using network and electronics diagrams from an engineering viewpoint to a simplified architectural stage of telecommunications.

2.1 Description of the SHAM chip

The technology incorporates in its circuitual fabrication or anatomic phase,

————— *Firstly*: the substrate possessing layers of sapphire insulation; subsequently, in the super-helical circuit's structure, one buffer layer out of two having GaN thus, resembling one pole of the combined switchable transistors to some HEMT heterostructure architecture, in principle. The air-core spatial aspect in measurement, explicates a free zone which does not allow the involvement of terminals expressed as gate, source or drain in the initial fundamental structure of transistors, here, containing quantum wells in the chip's structure. Therefore, one pole has a free zone Z ; let this be defined for the upper pole of this memory chip, and let the remaining pole (lower pole) be a Faraday effect zone of Z' , for this pyramidal circuit (see also Fig. 1.2, §1). Note that, the buffer in either pole shall remain consistent for any incoming data such that, the carbon nanotube sustains the best location of data at any point of data loss probable occurrence (escape of data flow or due to some technical problems on voltage bias), reciprocally. A substitution for the HEMT technology in this invention-model is proposed methodologically as MOSFET in aim of engineering 2DEG, where the latter is deemed to possess high transconductance measured in Siemens suitable

for common memory design and architecture incorporating CNTs (e.g., [6]). However, MOSFETs fail to candidate themselves as high memory devices discussed in [6], and the suggestion on an alternative solution is the current technology in the perception of HEMT and coiled CNTs embodied in this invention model. The prime agent to this solution is to use a catalyst, electric conductor and SiN_x , in regard to the insulating layer within the fabrication process. —————

————— *Secondly:* the installation grade of a pair of carbon nanotubes in some geometry of say, e.g., double-helix with resemblance to a helical antenna used in ‘plasma physics’, mappably. The links between their gaps (or, bonds) shall be given in terms of electron jump in its displacement between the nanotubes’ membranes measured in deca of angstroms or, $10\text{\AA} = 1\text{nm}$ multiplied by a scalar real number, $\tau \mid \tau \in \mathbb{R}$, for the occupying vector space. This measurement defines sizes of membrane strands’ nodal integration in a tensor manner for the electron jump at any point plausible, probabilistically. The result of this, allows an ultimate storage of data no matter the mutation course of some particle, in this case, an electron on any level of the permittivity state for this super memory. Furthermore, the notion of indices (n, m) as ‘chiral vector’, is not acknowledgeable as, $n = m$, representing the helix nanotube material as ‘purely metallic’ for CCNT perceived by Lambin *et al.* of [21]. Thus, $n \neq m$ is the most adequate in preserving a semi-conducting electrical property in practice (generalized by e.g., Lambin *et al.* in [21]). The junctions between CCNTs from one staircase step to another per catalyst, is of $(n, m); m - n = 3q$, where m, n and q are integers, showing the transition, metallic→semiconducting→metallic [39], forming in this case, a CNT diodic junction (see Fig. 2.1a, and [8]) done by a linear junction between armchair and zigzag. The CCNT diode junctions, ideally represent photovoltaic effect when the cavity for excited electrons reaches a thermal level above Fermi level measured in Electronvolts (eV). This effect occurs, once the excitation of electrons and their overall conduction process are in place, hence converting light into electrical energy. The conversion of light occurs, once the accumulation of energy valance begins to perform quasi-Fermi levels (or, the sum of quasi-quantized energy states) for the majority and minority of carriers, mobile within the cavity’s environment. —————

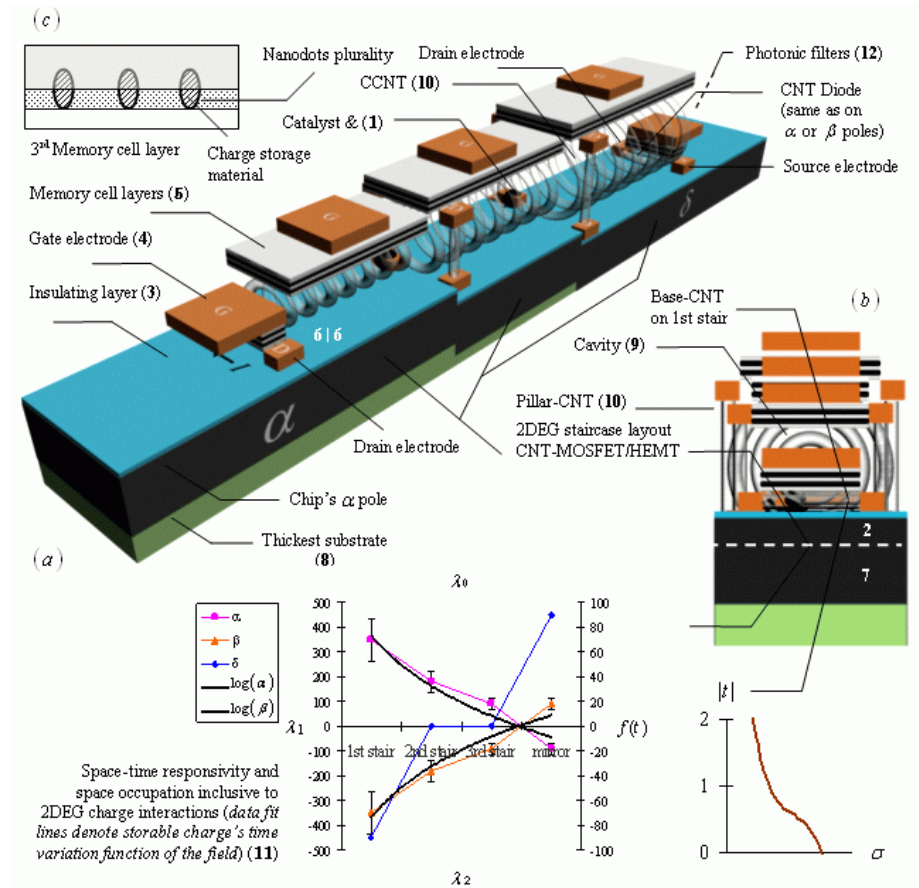
In contrast to CCNTs fabrication, the growth direction of pillar-shaped CNTs (observe Fig. 2.1) follows the direction of the electric field in the plasma enhanced chemical vapor disposition (CVD) process, discussed by Ren *et al.* in [32] and exemplified by Umeno *et al.* in [39]. In this case, even under high axial tension, CNTs should satisfy a vertical metallic interconnection course of integration whilst preserving a chiral vector value of $n = m$ or $(n, m); n - m = 3q \rightarrow 0$, as being an armchair type remaining metallic or, (n, n) discussed by Collins & Avouris in [9].

In continue, the threshold voltage V_{th} , increases versus one of the gate voltages when I_d remains constant, hence holes from the CNT are injected to the oxide-nitride-oxide (ONO) thin film between CNT and the gate electrode. It is deemed that from the electric field between each CNT and the gate electrode, the induced charge density σ , increases with proximity to polar CNTs of the chip (refer to the lower right graph of Fig. 2.1b), discussed by Choi *et al.* of [6]. Moreover, localized charge distribution enables charges to be induced into the nitride film of the ONO thin film due to the high electric field distribution from localized CNTs (Fig. 2.1c), and charges trapped in localized areas of the ONO thin film may be dispersed concerning drain current I_d , for either pole. This behaviour is normalized by utilizing metallic CNT adjacent to CCNTs, splitting the induced charge into different traps of the ONO as a choice of path for charge e (the continuation to this, is subject to §4). Hence, a CNT with a

diameter of 3 nm for an ONO thin film between the CNT and the gate electrode, being regarded as one single layer with an effective dielectric constant of 3, the calculated electric field for an applied gate voltage of 5 V would be, $970 \text{ V} (\mu\text{m})^{-1}$ [6]. In other words, the exemplified gate voltage forms a strong \mathbf{E} -field which is enough to induce a Fowler-Nordheim tunneling in the memory's CNFET application set using MOSFET technology. Furthermore, collapse of current or 'gate lag' problem is considered to be reduced between the division points. This reduction occurrence, is due to the proportional role of the CNT interconnection against CCNT in normalizing the electric current between the HEMTs from either pole, connecting source and drain electrodes to the gate electrode via contacting memory cell layer, simultaneously.

Before the depletion stage of current I_d , in its time response measurement for either pole as, $\alpha(I_d)$ and $\beta(I_d)$, the carbon Fermi energy in diodic points (contacts) occurs wherever CNTs join. These CNTs join each other with different electrical property (see nanotube joints and compare this with [8]), exhibiting quantized charges with sizes of $\leq 10 \text{ nm}$ at room temperature.

This type of quantization attracts structures for dynamic storage devices and data receivers in conventional computers and thus, resonators here as, e.g., super-RAMs and telecommunicators. The reason is the model's practical role for a real high to low p.d.-drag, defining the 'waterfall effect' in the chip's application.



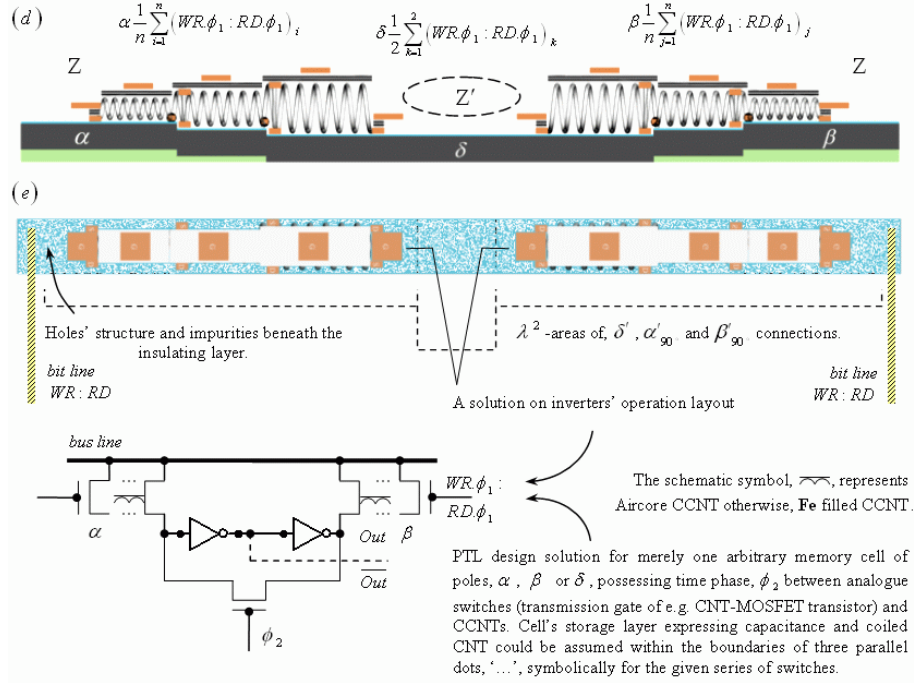


Figure 2.1 (a) A three-dimensional perspective view; (b) cross section view including a 4-dimensional chart of charge interactions between poles and 2DEG layering, with; (d) a complete pyramidal view of the involved poles of the general design; (e) top view of (d) plus a diagrammatic solution over the chip. The displayed components in representation are sectional to the design created by the author whilst; the layering and dimensions of electrodes could obey models of Choi *et al.* [6]; Krämer *et al.* [19] and Okita *et al.* [26], in description; (c) represents the memory layer nanodots to store data discussed by Choi *et al.* [6].

The diode-contacts mentioned formerly, denote the ‘voltage drop versus increase at the ends of the circuit in compensation’ from both sides i.e., the cyclical state of electric current from either pole as, $\alpha(I_d)$ or $\beta(I_d)$, correspondingly. The prevention factor on electric current coming from either CNFET with their base-CNT, is to prevent leakage problems thus acting like valves in-between α and β of the chip. Nevertheless, once the overflow occurs, the voltage drop on one side, does not mean the loss of data since on the other side, as the other CNFET pole, provides the same data from drain electrode reversibly. This is due to the structural representation and orientation degree of the CCNTs and catalysts.

The following is in conjunction with Fig. 2.1a materials and components as pointed out by number, i.e., a mere theoretical embodiment of the invention-model, where this integrated conducting/semiconducting device set is comprised of:

- 1- Copper (Cu) gate as a conductor from HEMT-to-helix or core and vice versa (the second as ‘helix’ or coil, is done by priority for the privileged places to store electrons, otherwise, it is the prioritization of the conduction grade of electrons).
- 2- Unintentionally doped (UID) AlGaIn. The thickness size varies from, $\theta \in (6.67 \text{ nm}, 25 \text{ nm}]$, in the layer’s geometric

space measurement for its staircase thickness, based on ratio $\theta_2 : \frac{\theta_1}{2}, \frac{\theta_1}{3} : \theta_3$ wherefrom left as middle to right as minimum- θ , represents ratios, 2nd:1st and, 1st:3rd descending stair, respectively.

- 3- SiN_x insulating layer within the staircase core of the PTVD-SHAM Chip.
- 4- Gate: Titanium (Ti) or Gold (Au). This applies to thick gates' principles for width and length measurements.
- 5- Memory cell e.g., (SiO₂/Si₃N₄/SiO₂) with a thickness of ~28-30 nm.
- 6- The symmetry of MOSFET/HEMTs as 'upper pole' (frontal portion is the memory cell).
- 7- Unintentionally doped (UID) GaN buffer layer. Size: 1 μ m for its thickness.
- 8- Sapphire substrate symmetric to MOSFET substrate, is for stable current against alternate current (AC) between terminals and the incorporated CNTs of this chip which possess high electrical conductivity (recall pp. 11 and 12). The thickness of this layer varies up to 350 μ m.
- 9- Cavity layer inclusive to the paired CNTs between the base terminals.
- 10- A novel mechanism representing electro-migration and multilevel metallization, here for vertical metallic interconnection (purely metallic CNT pillar construct with a chiral vector value of $n = m$, e.g., pillar-CNT, part *b*). This mechanism basically appreciates the model and utilization layout claimed by Greenberg *et al.* in [15]. Methods for bundling the pillar-CNTs attached to the staircase electrodes using electrophoresis, is claimed and discussed by Kim *et al.* [16]. Despite of number of turns, a CCNT in association with pillar-CNTs has tube and coil's minimum diameter of ~30 nm and 300 nm, respectively, with a theoretical inductance measured in micro-Henries.
- 11- A 4-dimensional chart of space-time charge interactions for all poles; spatial axis λ_1 is measured in microns and, λ_0, λ_2 , as maximum-to-minimum geometric length units of (1.11), where Hertzian concentration of 2DEG by time function $f(t)$, is measured in Hz. These considerations are satisfied by logarithmic interactions between poles, where the spatial occupation multiplied by time-fractal t^{-1} , generates the speed of interaction-mean for the circuit's total charge. Delta pole, δ , is $f(t)$ -dependant evaluated by time phase ϕ_2 , compared to pole's lambda spatial property.
- 12- Zone Z' , serving the optical buffer and relevant micro-filters explained earlier on pp. 14 and 15, §1; debates on the conditional planar or architectural extensions to the chip's poles.

2.2 Principle paradigm to satellite communications and self-clocking systems' engineering

The paradigm submitted as Fig. 2.2, instantiates in its design, our solar system's Sun thereby, justifying the accurate information-gathering on self-clocking systems, frequency of the state of data-time versus time-data depository under any circumstances. The given specification is also inclusive to the nature of travelling astronomical systems related to humans and probes in space in regard to planetary solar system missions and beyond, when applicable. In the process of data construction after being received, depending on what type of instrument one uses to observe objects, in this case say,

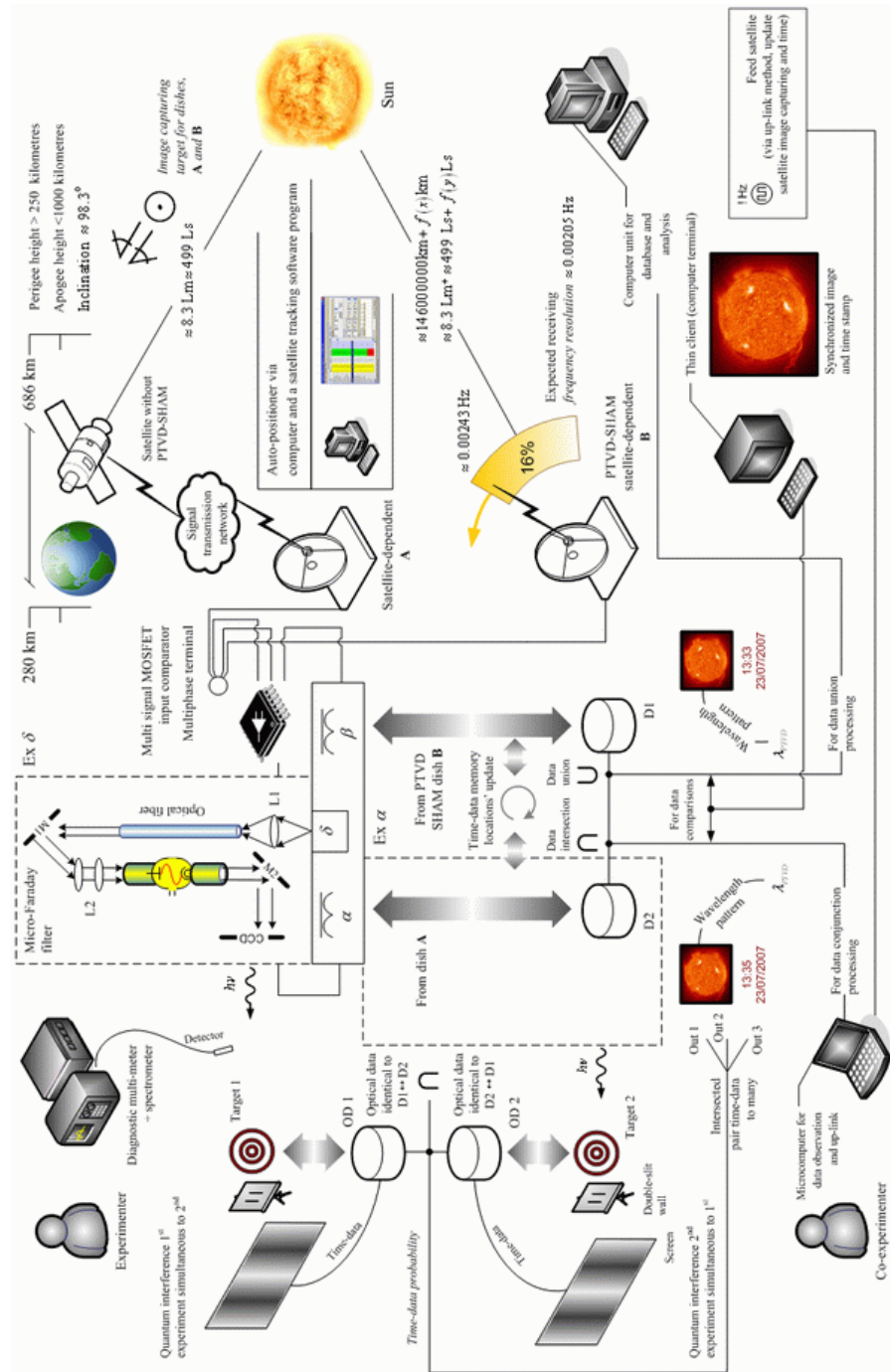


Figure 2.2. A view of PTV-D-SHAM paradigmatic network, engineering and task progress in efficiency modeling. All relationships between components do describe iterative methods

of the application in release.

e.g., a satellite system without PTVD-SHAM technology (Paradigm 2.2), an optical telescope autonomous of satellite (Paradigm 2.3), are being compared with a satellite system having a PTVD-SHAM unit mounted on its body.

The diagram describing paradigmatic relations between PTVD-SHAM components and their extensions, consists of engineering components such as micro-Faraday filters, Multi-phase terminal for incoming frequencies or transmissions and extensions of α denoted by, Ex α , in Fig. 2.2; refer to the given comments and call-outs' descriptions per electronics component or in general, per device package. The device package mostly includes an electronic otherwise, optoelectronic device components. In addition, kernel telecommunications systems as stationary e.g., PTVD-SHAM unit; semi-stationary e.g., satellite dish, which may displace for better receiving location point and dynamics, e.g., an artificial satellite orbiting earth.

Now assume an ordinary satellite without the consideration of a PTVD-SHAM captures images from the Sun. It is computable on the incoming streams of image data for say, a minimum distance from Sun (≈ 146 million km) in respect to the average and maximum distances to Earth, to consider a set of databases and PTVD-SHAM's multi-processing unit installation. Such processes could also be contemplated for analogue-to-digital conversion (ADC) stage, such as incorporating signal comparators [52] where the PTVD-SHAM unit remains for frequency resolution comparison issues.

Furthermore, digital logic in cases of PTVD-SHAM, obeys quantum property of interference experiment due to the utilization of micro-Faraday filter indicating the importance of compared streams of information in duality; i.e. reasoning particle duality, articulated in §4 via Tab. 4.1. It is factual upon these data comparisons, mounting digital cameras or CCDs supporting compressed images e.g., *.JPEG method would eliminate Hi-resolution image data. However, 'signal comparing' is most advised to be taken into consideration during the process for precise achievements in data-time recordings, e.g., D1, D2, and them amalgamating into D3.

Note that, in the above-mentioned distances between Earth and Sun, maximum, minimum and average distances including their remaining result of their difference, are represented with distance function $f(x)$. Discrete area function for frequency is given by $f(x, y)$ indicating ν covering this area for data access and thereby receiptment of information i.e., loci traverse. It is in that state, the function conceives the form, $f(x, y)_{\text{receive}}$, whereas $f(y)$, relates to measurements in light minute (Lm) satisfying a time-data jump (or Δt) by the following probability function. See the statement and Eq. (2.3) given on the next page. For simplicity, we take into consideration the minimum distance in realization of $f(x)$ existence.

—————*Time-data probability* in Fig. 2.2, represents a time-data jump from quantum state $t\delta \circ \psi$, to a new state $t\delta \circ \phi$. A quantum relation representing this type of probability could be expressed as,

$$\left. \begin{aligned} \text{prob (time)} &= \\ \text{prob (} f(t) \text{)} &= (t \circ \psi \Rightarrow t \circ \phi) = t \circ |\langle \psi | \phi \rangle|^2, \text{ and,} \\ \text{prob (data)} &= \\ \text{prob (} f(\delta) \text{)} &= (\delta \circ \psi \Rightarrow \delta \circ \phi) = \delta \circ |\langle \psi | \phi \rangle|^2 \end{aligned} \right| \prod \nu_{\text{bit}} = \frac{\delta}{t\delta \circ |\langle \psi | \phi \rangle|^2} \text{ in !Hz} \quad (2.1)$$

wherein consequence appreciates ‘general quantum interference’ given in [27, xviii]. In abstract algebraic terms of mapping and mappability, these mappings and time-data’s quantum-to-classical transition are determinable within the probabilities upon time and data functions respectively, or, $\text{prob}(f(t))$ and $\text{prob}(f(\delta))$. These time-data probabilities denote that the expected time-data from (1a), §1, representing the relationships of paradigm components. The ‘time-data expectancy’, emphasizes onto the product of time frame and data frame, both being updated iteratively (iterative method [27, xix]) for the involved devices in practice. The simplified form of relation (2.1) could be submitted as,

$$\therefore \text{prob}(\text{time.data}) = \text{prob}(f(t\delta)) = (t\delta \circ \psi \Rightarrow t\delta \circ \phi) = t\delta \circ |\langle \psi | \phi \rangle|^2 . \quad (2.2)$$

In essence, the latter must also appreciate the product restriction made on ν_{bit} in relation (2.1). —————

The example depicted in Fig.2.2 denoting 16% progress, indicates the receiving state for both imagery data including ‘time’ wherein return, treating this progressing state of frequency in approaching a perfected technology, one could compute on the given example,

$$\text{if } f(x, y)_{\text{receive}} \text{ for } \varepsilon \circ \lambda_{\text{PTVD}} = 16\% \Rightarrow \varepsilon = \frac{16\% \times 8.3 \text{ Lm}^+}{100\%} \approx 1.33 \text{ Lm}$$

then for the updated time frame, it is thus obtainable

$$\Delta t_{h,m,s} = 13 : 35 - 00 : \{1.33 \text{ Lm} \times c^{-1}\} \approx 13 : 33 : 40,$$

$$\text{where } (0.67\text{s} \times 60\text{s})100\%^{-1} \approx 40 \text{ s}. \quad (2.3)$$

The obtained time-stamp (refer to Fig.2.2) denotes: ‘Compared with the ordinary time measured on the Earth’s surface, this time-stamp thus articulates events of past being captured in an image as same as the expected image at Earth’s time, here given as 13:33 against 13:35 on the same date.’

On the one hand, the bidirectional database, $D1 \leftrightarrow D2$, collects relevant information on the time-data parameter as formatted in *more-precise* hours, minutes and seconds for $\Delta t_{h,m,s}$ in (2.3). Then it is calculable for the more-precise time-data event occurrence, the measurement of the displacing frequency proportional to the expected percentage for 16% of the frequency resolution is deduced as follows

$$\nu_{\Delta\omega} = \frac{c \times 100\%}{146000000 \text{ km} | f(x) \times 16\%} \approx 0.0128 \text{ Hz}. \quad (2.4)$$

On the other hand, the most-precise time-data frame can be accomplished once an updated technology based on PTVD-SHAM architecture is being introduced for its both: the electronics and optics as specified in Fig.2.2. The ‘most-precise time-data event occurrence’ in higher percentile is exemplified in Fig.2.3, §§2.3.

Nevertheless, with relevance to (2.4), bringing closer the collected data from a destination object, in this case ‘a stellar-like body’ e.g., our Sun to the source where a sender/receiver PTVD-SHAM unit is resided. This is the main objective yet to be accomplished. Notation $\nu_{\Delta\omega}$, stands for time-dependent frequency resolution which is not of a typical type frequency resolution in the principle of electronics. It is studying it in terms of: *the more closer scope of events to far destination, the more noise and superposition*. This is conducted by a sender/receiver unit after receiving imagery

data, using filters in the unit's structure in aim of adopting the close captured image of destination, into a normalized expected image as one captures in the point of satellite from the object in the point of destination. The 'time-dependent frequency resolution' means that, the performed frequency resolution is directly dependent to Heisenberg's uncertainty principle of quantum mechanics defined for time-frequency resolution as it should be [55], or,

$$\Delta\omega\Delta t \geq 2\pi$$

where the latter maintains an anti-distortion coming from divergence ($1/t$) contrasted to the context of time-frequency resolution for a Z transform method [55]. Quantity, $\Delta\omega$, represents bandwidth related to seismic waves, and for the present paradigm, relates to shock waves and other displacing/propagating waves including plasma waves near e.g., stellar objects [27] like our Sun. In other words, PTVD-SHAM technology could also be used for earthquake occurrences, which do have an uncertainty given by the duration of shaking, Δt , before earthquake mantle reach (upper or lower mantle layer of Earth) event occurrence! This proclaimed property of PTVD-SHAM satisfying seismic waves pre-event reach to Earth's surface as an earthquake, is due to the characteristics of parallel time t_{\parallel} , discussed in §5.2, in accordance with the characteristics of the displacing frequency proportional to the displayed percentage for the expected frequency resolution.

The result of close capture or scope displacement of the frequency in transmission, (2.4), would be a data frequency enhancement on the frequency's configuration and resolution, and is for imagery and photo-analysis purpose satisfiable by setting up a pair of quantum interference experiments. These optical data comparisons via quantum interference shall manifest the receipt of solar images in shorter lengths of time compared to the usual course of recordings. In the given paradigm, this change of time length is due to the nature of Gaussian curvature scenarios expressed in Tab. 4.1, §4 on charge, e , and greater curves in general relativity measured from Earth-to-Sun.

2.3 Sample paradigm to simple architectural implementation

This diagram consists of post-fabrication phase of the PTVD-SHAM chip and its peripherals e.g., steerable microwave antenna, portable geo-sample analyzer, solar charging panel and ... The basic specifics are given in Fig. 2.3. It is aimed for this 'device package' to represent an electronic and optoelectronic characteristics. In this sample paradigm, future interstellar telecommunications are envisaged to promote satellite communications in a robust manner. It points out radical issues for certain considerations on data path and algorithmic processes when one studies data transmission events within the core of the architectural aspect of the PTVD-SHAM design and methodology. This sample illustrates the vital information needed to be transmitted between space systems here e.g., people on planet Mars say, e.g., an astronaut's base and other necessary systems in their habitable complex prior to their geological sample gatherings and experimentation. We assume this level of technological accomplishment on the surface of Mars to be, when people could be said to use martian materials for their water, oxygen and other necessary life supplies.

So, any crucial information being transmitted between the planets, Earth and Mars stations, is thought to be resolved by PTVD-SHAM mother units that are at that point, quite capable of almost instantaneous data transmission between people of both planets due to the behaviour of frequency resolution displacement $\Delta\nu_{x,\Delta\omega}$. Ergo, for a perfected technological upgrade of a PTVD-SHAM system, assuming the progression percentage over $\Delta\nu_{x,\Delta\omega}$ attains 96%, one could thereby compute

$$\varepsilon = \frac{96\% \times 8.3 \text{ Lm}^+}{100\%} \text{ to light minute} \approx 7.96800 \text{ Lm} ,$$

$$\therefore \Delta\nu_{x,\Delta\omega} = \frac{c}{146000000 \text{ km} - \left(\frac{7.96800 \text{ Lm}}{8.3 \text{ Lm}} \times 146000000 \text{ km}\right) | f(x)} \approx 0.051 \text{ Hz} , \quad (2.5)$$

hence, approaching 100% for $\Delta\nu_{x,\Delta\omega}$, the final outcome would result into,

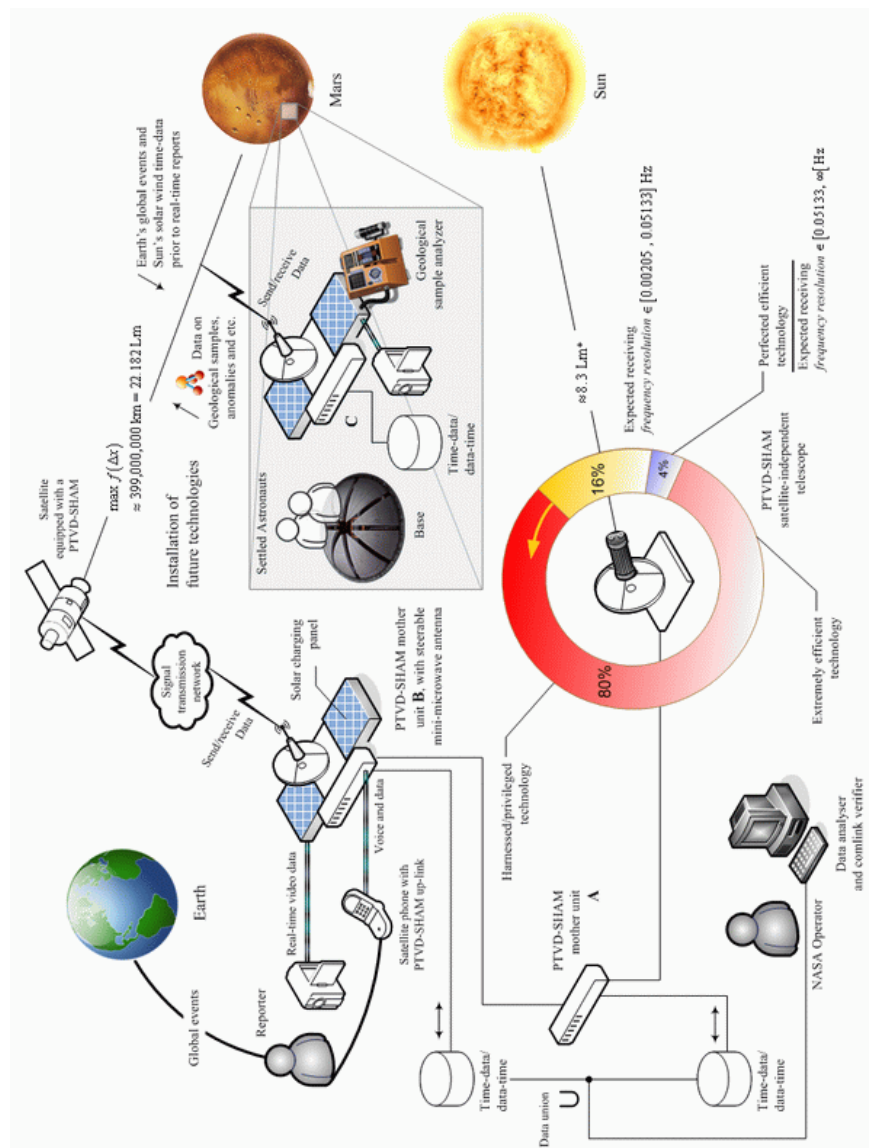


Figure 2.3. A paradigmatic network and upgrade modeling view relevant to Fig. 2.2.

$$\lim_{\Delta x \rightarrow \odot} \Delta \nu_{x, \Delta \omega} = \Delta \nu_{x, \Delta \omega} \in [0.051, \infty[\text{ , } \odot (\ll 146 \text{ million km .} \quad (2.6)$$

Let notation, \odot , represent Sun’s vicinity in terms of some close distance to the Sun, and Δx for the given limit, represent the change of distance for frequency resolution displacement $\Delta \nu_{x, \Delta \omega}$ maximally to \odot , according to the assigned limit.

This seems conclusive, especially when the capture of imagery/non-imagery events gets closer and maximum in range as possible to the stellar object and in other issues, non-stellar objects. Therefore, in this range, the noise state of frequency becomes obvious, where it deduces the following postulate benefiting from the previously articulated interpretations on paradigm results (2.4), (2.6), and probability relation (2.2),

Postulate 2.1. *for any device that captures events of a system of source as an object or body, the more closer scope of events to far destination representing frequency resolution displacement $\Delta \nu_{x, \Delta \omega}$, the more noise and superposition of information.*

3 Functions, operations and data analysis

With resumption of the issue submitted in §2, it is also imperative to consider in the following, the basic dependencies of the PTVD-SHAM chip i.e. terminal elements of PTVD-SHAM project (for more information, see issues given on project management e.g., [27, xii]), in terms of

- Firstly: PTVD-SHAM’s functions and operations as prior formulaic and structural frame of the application’s engineering point of view.
- Secondly: conducting the functions and operations as PTVD-SHAM’s first basic dependency and of course, the ‘chip’s description’ given in §2, on the basis of simulation grounds; thus leading to the final ground of experimentation and data collection with essential comparisons between the two grounds mentioned.
- Thirdly: cost estimation and project management for the experimental phase, which is not discussed in this paper; reasoning that, this terminal element solely represents the items that are cost estimated in terms of money-orientated resource-requirements, budget, duration constraints linked to timetables and other dependencies mentioned above.

Hence, it is currently prioritized to concentrate upon the first two dependencies. From there, future reports concerning ‘finance’ are to be annexed to this topic satisfying up-to-date events of the pre and post-fabrication phase of the chip and its peripherals. (Observe Figs. 2.2, §§2.2 and 2.3, §§2.3, respectively.) It would be sensible to propound the final cost estimation for the pragmatics phase rather than the theoretical phase, where the latter chiefly deals with the physical and engineering aspects of the problem at hand. The third dependency however, would be debated on the financial grade when the launching stage of the project based on paradigms of Figs. 2.2, §§2.2 and 2.3, §§2.3, including cost estimation models [27, xiv], are both considered in practice.

Nevertheless, it is predicted at this early stage, cost overrun or in this case, ‘budget overrun’ is not in the whole picture; since the compact design and accessories aiding the project are for now, treated in discrete. Ergo, a thorough investigation for these external/internal factors (environmentally and componentially-related to the chip), is needed to vindicate the affordability subsequent to the feasibility stage of the project.

As the matter of fact, it is gaining the permission of the usability issue on ‘external factors’ such as: artificial satellite systems, robust signallers and satellite dish, which at that stage is the main concern on the ‘cost overrun’ issue. For now, this ‘cost overrun’ as a constraint remains trivial against the semiconductor’s package on its basic promising technology. This is outlined in terms of the chip’s plausibility over ‘functions, operations and data analysis’ reaching the acme of its implementation versus budget constraints.

To this account, this Section acts in accord with §§3.1 and §§3.2 notes; whereas the latter is an example on the theocratical analysis achievable on databases layout given in §§2.2, §§2.3; whereas the former, commences with the chip’s basic functions and operations, essential to the chip’s future technology and database system as follows:

3.1 Functions and operations

The time-varying & data super helical access memory (PTVD-SHAM)’s main functions, satisfying a state of conservation of all classical Boolean logic & image-logic states, in a non-volatile versus volatile mode, conversely, is categorized and conceptually assigned by

1. Incorporating HEMT and MOSFET Logic for memory layers.
2. Incorporating, waterfall wave filters, here as time-purposed crystal oscillators; a combination of CCNT and Capacitors as series band-pass filters to form a passageway of normal frequencies between I/O, thus attenuating frequencies outside the range during operation with an advantage of freedom of choice of precise time and location for data. This type of oscillation would be more advanced than say, e.g., crystal momentum conserved in interactions between electrons and phonons in a crystal [18].
3. Integrating catalysts for best conductivity, reducing complexity on CCNT configuration as synthesized between catalysts at specific staircase sites. This is for regularizing the black body effect i.e. an object that deflects and thus controls energy accumulation by distributing it into other layers of adjacent waterfall chambers. The energy distribution prevents ‘thermal radiation overlapping’, including the conversion of photonic states of data into charge states of data.
4. Satisfying cavity’s quantum property via pillar-CNTs, memory cells and coiled CNTs as CNFETs and CCNT-FETs, respectively.

The operation module that involves the electro-migration throughout the functions mentioned above, for the circuit’s electronic components would then associate to operational conductivity problems as follows:

————— Once the delivery of electrons to the drain electron is made from the polar layers and the base carbon nanotube, it is then considered the mobility of electrons between the helical carbon nanotubes averaging between the highest mobile electrons (ballistic transport of hot electrons in the 2DEG layer according to relation 1.2, §1), as the ones attaining the soonest. In return, the typical electrons being conducted via base-CNT therefore, are considered the soonest otherwise the last ones in arrival. Hence, the delayed charges of electrons (holes) are stored to the memory cells’ last addresses or the farthest memory location to base-CNT (or, 1st rising stair, where biggest helical CNT resides). Consequently, the soonest ones in terms of first-in-first-out (FIFO) are the ones already stored in the memory cell’s address e.g., leftmost

part of the upper pole's wafer construction against the notion of the first popped-out data in the rightmost part of the upper pole's wafer. This is done when writing data operation is enabled via PTL logic setup. —————

This type of conduction, prevents latency and other problems in accessing data by averaging the time of data-dispatch, store and access, now prioritized as: 'Where is best to deposit data pre-per second'?

This so-called 'pre-time attribute' is forwarded for a pre-optimized prior location and time for data being stored and thus accessed functionally/instantaneously via helical CNTs. The time-data accessibility is a resolved issue due to the existence of the helical structure of the incorporated-paired CCNTs. The mutual conductance or transconductance as described in the previous paragraphs on late and early carriers here, electrons, from both HEMT poles to the centre (or, the staircase where helical CNTs embed in), is calculated by

$$\langle g_m \rangle_{\alpha,\beta} = \frac{1}{j} \sum \frac{\Delta I}{\Delta V} \text{ for } \alpha \wedge \frac{1}{j} \sum \frac{\Delta I}{\Delta V}, \text{ for } \beta, \text{ such that,} \quad (3.1)$$

$$\begin{aligned} \langle g_m \rangle_{\alpha,\beta} &\equiv \frac{1}{j} \sum_{i=0}^{j \geq 2} \left(\frac{\Delta I}{\Delta V} \right)_i = \frac{\Delta I_{ds,CNT}}{\Delta V_{gs,CNT(\alpha,\beta)}} = \frac{\Delta I_{ds} + (\Delta I_{CNT_1} - \Delta I_{CNT_2})}{3\Delta V_{gs} + \Delta V_{CNT\beta} + \Delta V_{CNT\alpha}} \\ &= \frac{g_{m1} + \Delta g_{mCNT}}{2}, \end{aligned} \quad (3.2)$$

where the latter and former relations initially come from the transconductance formula in field effect transistor's general cases, parametrically,

$$g_m = \left. \frac{\Delta I_{ds}}{\Delta V_{gs}} \right|_{V_{ds}=\text{constant}}. \quad (3.3)$$

As if said that, the distribution in (3.2) for the electric current is expressed by $\langle g_m \rangle$, which is the distributed ratio of all current, I , on the output port between the 'helical CNTs and electrodes' as, $\Delta I_{ds,CNT}$ and, $\Delta V_{gs,CNT(\alpha,\beta)}$, denoting that all voltages on the input ports of the source and gate electrodes, are followed by base-CNT voltage, $V_{CNT\beta}$ and $V_{CNT\alpha}$, in terms of, $\Delta V_{gs,CNT\beta}$ and $\Delta V_{gs,CNT\alpha}$, respectively. Hence, for both poles in respect to their carriers' current direction with respect to their p.d. occurrence, therefore, relation (3.2) becomes the most privileged in practice.

3.2 An example of data analysis on PTVD-SHAM application

Suppose one acquires the basis of technological specifications of the PTVD-SHAM chip as described in §2, and its completion of its anatomic phase and mechanism of the chip. Phases of data analysis, error reporting procedure and experimentation after successful attempts in the laboratory, requires Kirkup's experimental methods in specifying the data points in form of spreadsheets and graphs, as exemplified [17, pp.168-172]. By means of which, voltage V , I/Os e.g., linearization of the voltage function [27, xxiv], performing relationships between V and electric current I for the PTVD-SHAM device, is a necessity in establishing explicit data analysis. These parametric relationships in some other graphs, should also represent events of time-data/data-time in form of, data \circ time \circ data, against voltage V , otherwise current I -values on x - y axes of the chart/graph. The storage process and property on the 'events of time-data/data-time', is subject to §4, §5, and Major to §§5.2.

After accomplishing these basic technological requirements and submitting a report documentation, the experimenter thereby lays out the abilities of the technology in virtue of data anticipation and self-clocking system for e.g., radar systems. The expected data on this promising property of the device, can be plotted and spread into a radar graph and x - y standard charts. The database dedicated for data analysis should contain data satisfying parameters $f(x, y)$, t , ε , Δt , $\nu_{\Delta\omega}$, $\nu_{\Delta\omega, x}$ of the PTVD-SHAM system in its attributes. Here is one worked out example:

$f(x, y)_{\text{receive}}$ (%)	Lm	t (minute)	ε (Lm)	Δt (minute)	$\nu_{\Delta\omega}$ (Hz)	$\nu_{\Delta\omega, x}$ (Hz)
1%	8.3	1	0.083	0.917	0.205479452	0.0020756
2%	8.3	1	0.166	0.834	0.102739726	0.0020967
4%	8.3	1	0.332	0.668	0.051369863	0.0021404
8%	8.3	1	0.664	0.336	0.025684932	0.0022335
16%	8.3	1	1.328	-0.328	0.012842466	0.0024462
32%	8.3	1	2.656	-1.656	0.006421233	0.0030218
64%	8.3	1	5.312	-4.312	0.003210616	0.0057078
70%	8.3	1	5.81	-4.81	0.002935421	0.0068493
80%	8.3	1	6.64	-5.64	0.002568493	0.010274
90%	8.3	1	7.47	-6.47	0.002283105	0.0205479
96%	8.3	1	7.968	-6.968	0.002140411	0.0513699
99%	8.3	1	8.217	-7.217	0.00207555	0.2054795
100%	8.3	1	8.3	-7.3	0.002054795	#DIV/0!
1%	3.1	1	0.031	0.969	0.053800661	0.0054344
2%	3.1	1	0.062	0.938	0.269003303	0.0054899
4%	3.1	1	0.124	0.876	0.134501651	0.0056042
8%	3.1	1	0.248	0.752	0.067250826	0.0058479
16%	3.1	1	0.496	0.504	0.033625413	0.0064048
32%	3.1	1	0.992	0.008	0.016812706	0.0079119
64%	3.1	1	1.984	-0.984	0.008406353	0.0149446
70%	3.1	1	2.17	-1.17	0.007685809	0.0179336
80%	3.1	1	2.48	-1.48	0.006725083	0.0269003
90%	3.1	1	2.79	-1.79	0.005977851	0.0538007
96%	3.1	1	2.976	-1.976	0.005604235	0.1345017
99%	3.1	1	3.069	-2.069	0.00543441	0.5380066
100%	3.1	1	3.1	-2.1	0.005380066	#DIV/0!

Table 3.1. Estimated values on attributes $f(x, y)$, t , ε , Δt , $\nu_{\Delta\omega}$, $\nu_{\Delta\omega, x}$, gathered in a spreadsheet for the PTVD-SHAM in use on Earth i.e., gathering information with pristine anticipatory abilities on the time factor t (assumed it, a 1 minute duration limit), in terms of its quantum jump via Δt , from the Sun §§2.2 and planet Mars. For ‘Mars’, herein hypothetical assumptions on tuple values have been worked out.

As one perceives from Fig. 3.2(b) pertinent to the spreadsheet, the ‘radar chart’ would be the most appropriate representation of sending/receiving data points of hertzian statistics upon $\nu_{\Delta\omega}$ and its displacing type oscillation $\nu_{\Delta\omega, x}$ from Eq. (2.4). By paying attention to the 5th and 6th tuples (database rows) in Tab. 3.1, one could simply determine that a mutation course arrives in-between 8 to 16% of the function $f(x, y)$ attribute (database column). Therefore one deduces that, ‘this mutation course of time’ as Δt , is due to the events of frequency ν , accessing ranges of 8.3 light minutes (Lm) for ε , on the distance measured between Earth and Sun in our solar

system. A similar scenario and hence its interpretation is applicable to the Mars case commencing with tuples 14 to 26.

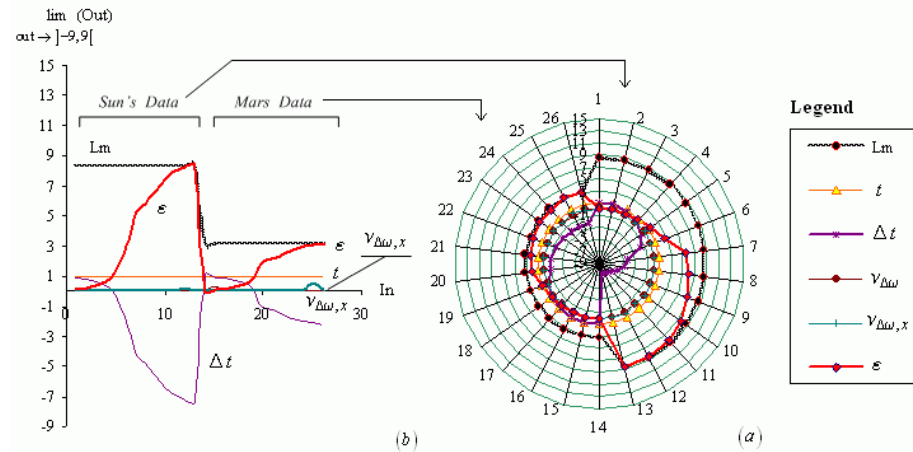


Figure 3.2. (a) A radar chart generated from Tab. 3.1.’s spreadsheet set up in Microsoft® Excel© XP; * (b) One *wide open* and one *fastened dental plier effect* as right and left nodes respectively, forming a flatfish via the involved parameters ϵ and Δt including their curves fall and loop. Other parameters for their curves are simply detected by referring to the legend.

So, the events as such, denote a mere presence of frequency resolution displacement $\nu_{\Delta\omega,x}$ for the progressing factors in terms of percentages to the database denoting discrete area function of x and y for Δt of the database. Furthermore, the more input values (13^+ inputs in the example above), the more accurate in defining the efficiency factor of the technology. This forms a full circle proper to the output values limit and integration, as specified by the y axis in Fig. 3.2b. The full loop generated on either chart indicates values of ϵ being highly ascended and thereby attaining this geometric progression [27, xxv], covering and traversing greater areas of time change as time-data jump Δt . Compare this time jump (mutation) with Tab. 3.1 and refer to paragraph #4, p. 20, of §§2.2, including ‘*time-data probability*’ in the named Subsection. The full closure of the loop represents a 100% for $f(x, y)$, or a full success of the application which is the most perfected/privileged ideal state of the technology.

In Fig. 3.2(a), a *dental plier effect* with its minimal node of orientation, is what is expected from the time-data jump between Δt and ϵ mirror-growth of ‘geometric negative versus positive progression’, which obviously conserves states of quantum superposition and thus information noise according to Postulate 2.1. The mutation course and statistical comparisons between Sun and Mars data in the spreadsheet, proves further the ‘*far destinations*’ scope of events mentioned in Postulate 2.1. The same count applies to other distances of $(f, x)_{receive}$, whereby the effect in its data point population is more completed for the effect’s curves proportional to the number of inputs given in the database system.

The spreadsheet data in Tab. 3.1, are performed into two consecutive quadrants each relating to paradigms of §§2.2 and §§2.2. Those are the examples given on Sun and Mars regarding the usage of PTVD-SHAM, which corroborates with paradigm

* Excel XP is a spreadsheet developed and distributed by the Microsoft Corporation of America.

result (2.6), and the basics of data value comparisons. The ‘#Div/0!’ element of the table, denotes the ‘division by zero’ problem which is already given in the interval $[0.051, \infty[$ for $\nu_{x, \Delta\omega}$ of the mentioned equation result. The connectivity of *nodes of dental pier effect* from one to another, forms shapes of e.g., a ‘flatfish’ as generated via the spreadsheet software program. This demonstrates a state of continuity on PTVD-SHAM’s componential functions, whilst quantum states of $\nu_{x, \Delta\omega}$ via ε being conserved as discrete areas of $f(x, y)$, traversed for all nodes and loci under the curves of the effect (its integrals). Hence, the range of percentages upon areas of the function stipulates for the device, conditions of hierarchical loci access of information and walking through node by node of data, which is either pre-ordered or post-ordered i.e., being traversed.

4 The role of Gaussian curvature and the concept of electrons in B-field normal to external E-field via Maxwell-Lorentz theory in Minkowski’s space and time universe

In cases where in the field of induction, a study of an electron in motion with alignment to the S and N poles of the CCNT is being prioritized, the study of other bodies as mobile electrons coming from quantum confinement in HEMT cases, are too reciprocally prioritized in product terms. The variations of energy states with the external fields are reflected in the electrical and thermal conductance of the CNT with chiral vector unit $n = m$. The CNT as ‘pillar CNT’, is vertically constructed between the electrodes of either pole. The number, the heights, and the positions of the conductance peaks, are strongly dependent on the external fields where **B**-field and **E**-field are visited. This condition is satisfied by the following electromagnetic process initially elicited from the theoretical notion of Minkowski’s space and time,

$$\mathfrak{E} \equiv \left(e\sqrt{-1e_2e_2'} \right) \dot{t}, \quad -ee_1\dot{t} = \frac{\bar{\Sigma} \cdot \Sigma}{-ee_2\dot{t}}, \quad \bar{\Sigma} \equiv \frac{\Sigma_x + \Sigma_y + \Sigma_z}{3} = \frac{1_x + 1_y + 1_z}{3} = 1_\tau, \quad \Sigma = 1, \quad (4.1)$$

where \dot{t} , is the time factor equal to $\frac{dt}{d\tau}$, or simply, $\dot{t}^{-1} = \sqrt{1 - v^2c^{-2}}$, defining ‘relativistic time intervals’ between the storing events of data. Ergo,

$$\therefore \bar{\Sigma} \cdot \Sigma = 1_\tau \cdot \Sigma = e^2 e_1 e_2 \dot{t}^2, \quad \text{whereby, } \therefore \bar{\Sigma} \cdot \Sigma = 1_\tau \cdot \Sigma = \frac{e^2 e_1 e_2 \dot{t}^2}{1 - v^2 c^{-2}},$$

$$\therefore t = \frac{\tau}{\sqrt{1 - v^2 c^{-2}}} \text{ and } 1_\tau \xrightarrow{\frac{x_1}{ct_1} \wedge \frac{x_2}{ct_2}} \frac{\tau}{t_1}, \frac{\tau}{t_2} \text{ iff } \dot{t}^2 \neq \dot{t}'^2, \quad (4.2)$$

wherein this case $\dot{t}^2 \neq \dot{t}'^2$, obeys Russell’s Paradox (e.g., [31]; [34]) as a ‘free variable’ satisfying global time scenarios on the current frame of time ratios, due to the probabilistic existence of electron of the charge, e_1 for e of product $e^2 e_1$ and, e_2 for the same e of product $e^2 e_2$, in the context of simultaneity. Time, t of c in $\frac{x_1}{ct_1} \wedge \frac{x_2}{ct_2}$ as stationary time in (4.2), is due to the definition of speed of light, c , an invariant speed $\approx 300000 \text{ kms}^{-1}$. In other words, time entanglement of past, current and future events for data product value in terms of data constituent, hereby as, one entangled e in a probabilistic flow of entangled and non-entangled electrons (compare with quantum time entanglement of electrons [24]), could be expressed as,

$$\frac{dt}{d\tau} \neq \frac{dt \leftrightarrow \tau}{d\tau \leftrightarrow t} \text{ for } e \in e^2 e_1 \wedge e^2 e_2 \Rightarrow \therefore \dot{t}^2 \neq \dot{t}^2 \text{ for } e \in e^2 e_1 \wedge e^2 e_2. \quad (4.3)$$

Let time t in the ‘time dilation’ concept, represent relativistic time, and τ be the time at rest or ‘proper time’ being validly defined in Einstein’s theory of SR. Thus, specifying this proper time via implication relation elicited from 1_τ in (4.2) for bodies e_1 and e_2 , respectively, dilates

$$\therefore 1_\tau \cdot \Sigma = \frac{e^2 e_1 e_2 (t_1 t_2)}{1 - v^2 c^{-2}}, \quad (4.4)$$

$$\therefore \left(\frac{\tau}{t_1}, \frac{\tau}{t_2} \right) \Sigma = \frac{e^2 e_1 e_2 (t_1 \vee t_2)}{1 - v^2 c^{-2}}, \quad \dot{t}^2 \neq \dot{t}^2, \quad (4.5)$$

$$\therefore 1_{\frac{d\tau}{d\tau}} \cdot \Sigma = e^2 e_1 e_2 (t_1 \vee t_2), \text{ or, equivalently,} \quad (4.6a)$$

$$1_{1 \rightarrow (x,y,z)t'} \cdot \Sigma = e^2 e_1 e_2 t_1, \quad e^2 e_1 e_2 t_2. \quad (4.6b)$$

The previous relation generates a ‘Newtonian attraction’ in accordance with Einstein *et al.* [14] on the basis of two points of mass, m and m_1 , describing their world-lines satisfying cases relating to mm_1 in the context of Lorentz’s rest mass and relativistic mass of special relativity, correspondingly.

Let \mathfrak{E} represent an entanglement vector for electron charge e and e_2 relativistically. Body charge, e_2 , is deemed to be in confinement thus the notion of complex plane’s engagement in theory stands relevant upon e_2 .

In other words, the involvement of imaginary unit $i \equiv j = \sqrt{-1}$, in these previous relations explains the presence of at least one complex plane pertinent to the emanating field sourced from CCNTs.

Once the problem is discussed in terms of the point of confinement on e_2 to the actual point(s) of probable entanglement locus expressing e_2 and its symmetry e'_2 , as an entangled state of the same particle’s occupying space, the product of vector \mathfrak{E} thereby suits against proper time τ . Consequently, paradox $\dot{t}^2 \neq \dot{t}^2$, will emerge from this vector-form entanglement.

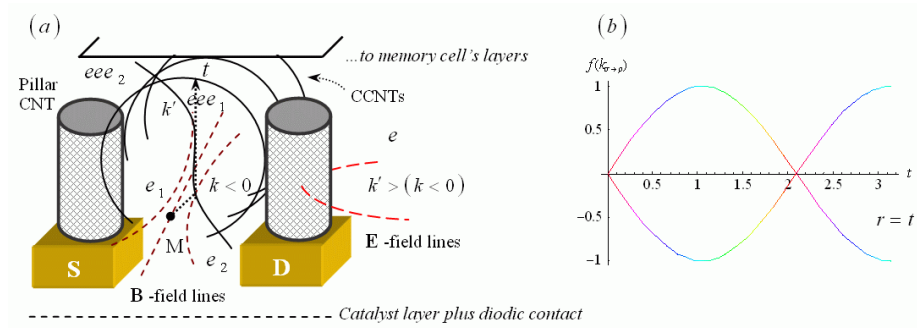


Figure 4.1. (a) The theoretical state of Gaussian curvature, $k < 0$, a hyperbolic geometry from the diametric viewpoint of the CCNT’s structure, from centre to circumference of the nanotube against $k' > (k < 0)$ inclusive to the charge and fields’ involvement; (b) curvature function, $f(k_{\sigma \leftrightarrow \rho})$, with an evolutionary quantum charge density, $\sigma \leftrightarrow \rho$ -index. See also, current Section’s items: † and ‡ on the subsequent pages.

† ————— *Operation:* the curves of Fig. 4.1a satisfy **B**-field and **E**-field loci where're therefore visited on charge e , in its electro-migration of $e^2e_1e_2$ on world-line at P and its symmetry P', for intersected charge e between curvatures $k' > (k < 0)$ and $k < 0$. This occurs when from the drain electrode, 2D hot electron migrates into the cavity region between first point electron and second point electron of charge e , as e_1 and e_2 , respectively. When the external hyperbola of the migration line reduces to internal hyperbola with centre M of the **B**-field lines, therefore, touching the world-line in P, achieves $\rho = \infty$ for magnitude $c^2\rho^{-1}$, relevant to the debate made by Einstein *et al.* [14] regarding space and time. So, the fields' interactions, permits their lines to form external curvatures in a magnitude of a displacing field which permits electro-migration on both sides of the curves at the magnetic polar points of the CCNT, such that, a selective approach (random) of the charge being stored in the memory cell becomes apparent. This selective approach for the involved charge is in manifestation, once the paradox, $t^2 \neq t'^2$, in subsequent relations sustains. This is due to the earlier vindication made upon the fields interaction course for all superimposing charges of e . The **E**-field lines radial to the cavity's core perform with a deflective course of eee_1 and eee_2 depending on **B**-field lines' polarity. The area of selective displacement of the charge is of elliptical volume otherwise spherical volume of space (see e.g., relation 4.18) demarcated between hyperbolic points of the fields. The eventual resultant on this particle(s) demarcation, produces 'image-logic patterns' of the stored charge in terms of Moiré pattern, submitted in relation (4.21). The selective superposition state could be amplified by the catalysts between CCNTs. Fig. 4.1b curvature function, $f(k_{\sigma \leftrightarrow \rho})$, with an evolutionary quantum charge density, $\sigma \leftrightarrow \rho$ -index, represents continuous charge density of total charge, Q , of Gauss's law over two-to-three dimensional worldline whose curvature expands and contracts spatial dimensions between **B** and **E**-field lines. This expansion/contraction of space dimensions is done via time line as radial time distance r , relevant to equation (4.18), introducing contour integral results, (4.10 and 4.11), as a follow-up on Fig. 4.2. The latter integration output, is adjusted for energy spectra satisfying the contraction and expansion grades of energy bands for storable and passing charges (or, transitory charges) between electrodes, cavity and memory cell layers. Colour representation of the spectra performs a relativistic Doppler shift effect (e.g., [35]) from the body during curvature's geometric transformation. The charge's mass condition by its energy state relevant to the evolution mentioned earlier (Fig. 4.1b), is given in Tab. 4.1. —————

‡ ————— *Operation's deduction:* it is by operation deduced that, the Gaussian curvature of $k' > (k < 0)$ against $k < 0$ from Fig. 4.1, for any problem involving all geometric conditions upon bodies in the **B**-field and active layers of the semiconductor (here as the 2DEG layer), remains intact to the notion of 1-bit logic against 2-bit logic. The latter bit form, equivalently in quantity, represents one qubit to the course of entanglement principle. This course of entanglement for one qubit, assumably occurs within the magnetic field prior to the particle's confinement. —————

At issue, the fundamental notion to confinement is of signifying $e^2e_1e_2$, which is always equal to storage vector, $\Sigma = 1$, cross product to its spatial Σ_x , Σ_y or Σ_z as a net storage product $\bar{\Sigma}$, such that 1, here, represents 1-bit in favour of some spatial dimension in form of Σ_x , Σ_y or Σ_z . The latter storage product is being fulfilled, once

the net direction of motion of e , e_1 and e_2 is clarified, i.e., when the ratio to the defined spatial directions is too evaluated, accordingly. This $\bar{\Sigma}$ is neither of velocity vector \vec{v} , nor must be confused with acceleration vector \vec{a} ascribed in Minkowski's space-time viewpoint, whereas, supposing that, arbitrarily one of the axes x, y or z e.g., by laws of delimitation on z approaching $z = 0$, eludes in form of

$$\lim_{\Delta z \rightarrow 0} \frac{1}{\Delta \tau} \tau \cdot \Sigma = 1_x \cdot 1_y = \log_{\Sigma} 1_{xy} = 2 \quad (4.7)$$

, forming a two dimensional cell, shall store data in favour of storage vector Σ for the exemplified dimensions x and y in two different stationary time scenarios, t_1 and t_2 of $dt \leftrightarrow \tau$, as follows

$$\therefore \Sigma^2 = \left\{ 1_{xy} = e\sqrt{e_1 e_2 e'_2 t_1} \left(e\sqrt{e_1 e_2 e'_2 t_2} \right) \right\}, \quad (4.8)$$

$$\therefore \Sigma = \left\{ 1_x = e\sqrt{e_1 e_2 e'_2 t_1}, 1_y = e\sqrt{e_1 e_2 e'_2 t_2}, 1_y = e\sqrt{e_1 e_2 e'_2 t_1}, 1_x = e\sqrt{e_1 e_2 e'_2 t_2} \right\}. \quad (4.9)$$

This eccentrically satisfies one of the spatial dimensions properly thus, articulating that e_1 , could also be entangled with e_2 , whilst having in position, e'_2 , once the product is emerged from $1_r \cdot \Sigma$. Therefore, e_1 , becomes well-vindicated in its spatial data depository characteristics for proper time interval, $dt \leftrightarrow \tau$, against the occurred time factor \dot{t} , and 1_{xy} , representing the normal to 'velocity vector' in the hyperbolic world-line which has been already occurred at the moment of depository's bitwise transformation.

Thus, such vectors normal to velocity vector are ignored since the occurrence of time factor \dot{t} from time function $f(t)$ for Σ , is prematurely simplified into τ_{Σ} with area coordinates' limit to (4.11)'s time-symmetries in say, some 'image logic'.

However, $\bar{\Sigma}$ could be understood with the analogy of Newton's second law, $\vec{F} = m\vec{a}$, defining 'effective mass' in crystals using quantum mechanics according to [27, x]. To measure the previous relations after the storage vector event occurrence on 1_x and 1_y , benefiting from relations (4.14a); (4.14b) and (4.18), explicitly,

$$\therefore \oint_A \mathbf{D} \, d\mathbf{A}_{(xy, x_i y_i)} = \int \frac{\Sigma}{\Sigma \rightarrow \Sigma^2 f(t)^{-1}} d\Sigma = \left\{ \frac{\Sigma^2 \tau_{\Sigma}^2}{1_{x,y} \rightarrow 2(xy, x_i y_i)} \right\} \quad (4.10)$$

$$\begin{aligned} &= \left| \frac{e^2 t^2}{2A^2 \tau^2} \right|_{xy | x_i y_i}^{x_i y_i | xy} = \left| \frac{-e_1 t_1}{\sqrt{2} xy \tau} \right|, \left| \frac{-e'_2 t_2}{\sqrt{2} x_2 y_2 \tau} \right| \\ &\equiv \frac{e\sqrt{e_1 e_2 e'_2 t_1 | t_2 t_1}}{\sqrt{2} (xy | x_2 y_2) \tau \int_P dj}, \frac{e\sqrt{e_1 e_2 e'_2 t_2 | t_1 t_2}}{\sqrt{2} (x_2 y_2 | xy) \tau \int_P dj} \text{ in } \text{sAm}^{-2}. \end{aligned} \quad (4.11)$$

where discrete valued area of $d\mathbf{A}_{(xy, x_i y_i)}$ is perpendicular to electric displacement field, \mathbf{D} in discrete axes of e 's movement between coordinates xy and $x_i y_i$, or by case in point to the latter, $x_2 y_2$. Discrete representation, $\left| \frac{-e_1 t_1}{xy \tau} \right|, \left| \frac{-e'_2 t_2}{x_2 y_2 \tau} \right| \cos\left(\frac{\pi}{4}\right)$ or $\sin\left(\frac{\pi}{4}\right)$, measured in sAm^{-2} or, Cm^{-2} , states that: Negative stationary time as 'stored time' from the 'past proper time' was once from either of complex plane integral of j , being multiplied into each other from both outcomes via depository vector Σ .

Let this integral be of the square root resultant for τ_{Σ} via an 'OR closure operator', or, $\bigvee_{i=2}^n i$. It is perceived that the remaining negative components in SR relation (4.13), resulting negative planer values by implying limit, $\lim_{P \rightarrow -\infty}$, under radical for P of the integral, could be any OR'ed value assigned to j in its summation form, $\sum j$, in the negatively progressing definite contour integral result.

The electron mass evolution process of, $\forall mv_e v_{e'} \in \prod E_{e \xrightarrow{L_V, R_V} \psi\rangle}$	Velocity-state; space-time scenario	Selective mass ratio as expanded or else, contracted mass against; stationary mass or its rest mass	Type of mass evolution (transmission technology)
$v_e \rightarrow v_{e'} < c$ $\therefore \Delta m_e = \gamma m_0$	$v < c$; timelike	$\Delta m_e = \gamma 9.109 \times 10^{-31} \text{ kg}$; $9.109 \times 10^{-31} \text{ kg}$	Hot electron (CNT-HEMT) or; typical hole (from CNT-MOSFET's 2DEG Layer)
$\int v_e v_{e'}^{-1} dv_{e'} \leftrightarrow c$ $\therefore m_0 = m_e \gamma^{-1}, \Delta m_e = \gamma m_0$	$v_{e'} > v_e \leftrightarrow v = c$; timelike \leftrightarrow null	$\Delta m_e = \infty$; 0 kg	Hot electron \leftrightarrow Photonic (PTVD-SHAM)
$\int v_e v_{e'}^{-1} dv_{e'} \rightarrow v > c$ $\therefore 2m_0 = m_e \int_P dJ^{-1}$	$v > c$; spacelike	$\Delta m_e = \arg(\infty) m_e$ $\in (-\pi, \pi] 9.109 \times 10^{-31} \text{ kg}$	N-dimensional complex plane selective (PTVD-SHAM) or; superluminal phenomenon

Table 4.1. Particle dynamics/kinematics evolution table. Symbol, ∞ , merely represents complex infinity argument by Krantz [20] depending on the body's mass state of selecting trap sites via radius of time $r = t$, exclusively (see Fig. 4.2). Symbol, γ , represents relativistic gamma from the theory of SR, whereas e' , is the theoretical counterpart of charge e satisfying far and close radial space and time distances between cavity and memory cell traps.

In other words, j 's sum by its assigned complex plane function is also independent of a choice of coordinates. This is given after enunciating the following hypothesis relevant to previous relation, complying with future relation (4.18).

Hypothesis 4.1. *Two explicit storage outcomes on computable data in a memory cell may exist as charge, e , in an n -dimensional space traveling in a bi-reachable path as length contraction/expansion via \sqrt{xy} advanced to the space area and volume occupation. The following proof by deduction, leads to the current hypothesis:*

Proof by deduction. *Two explicit storage outcomes on data for a super-helical memory cell is envisaged to exist as charge, e , given in (4.11) ready to be stored integrally, therefore measured in Coulombs per square meter when the depository vector, Σ , in closure, establishes stored time for either outcome. At the beginning, once the depository vector, Σ , establishes entangled time t in favour of entangled charge, e , equal to total quantum charge Q from (4.18), would therefore be in confined quantum entanglement on area A , as, $Q \sqrt{Q Q'} (2\sqrt{xy} A_{x_i y_i})^{-1}$. This type of confinement is for outcomes of (4.11) and (4.18), where $\psi(\mathbf{r})$, is Schrödinger's wavefunction, and time barrier $t_1 |t_2 t_1$, is the confinement operator on any occurring entanglement. This entangling area of total charge confinement, thus generates a volume of freedom of area of choice $A_{x_i y_i}$ for charge, e , via $\sqrt{Q \sqrt{Q Q'}} (2\sqrt{xy} \mathcal{V})^{-1}$, measured in Coulombs per cube meter multiplied by chosen meter. The \sqrt{xy} dimension is calculable by Lorentz transformations concerning length contraction, hereon the context of charge, e 's path bi-reachability as length contraction/expansion.*

Imperatively, the conduction of 'image logic' might to some people stand as a chronicle point for merely photosensitive materials and devices such as charged cou-

pled devices (CCDs) illustrated in Fig. 1.2, §1. Nevertheless, ‘image logic’ is a factual grade of computational processes, where one or more than one logic and image state, are combined into one data collection in release (Fig. 1.1, §1). In reason, the image logic’s output is of permitting a set of phenomena as bodies in motion and their entanglement on loop factors of time themselves in the context of simultaneity. That is, Einstein’s synchronization procedure by Einstein in [13], using Lorentz transformations on observable data path in expansion/contraction (proper length x' , when simultaneous paths for the body stands applicable with rise and fall of y'). The latter transformation is paradoxical to just, ‘length contraction’ recalled by Nave [25], and time, now into a proper-stored time τ_Σ , is proportional to proper time in Minkowski’s metric for relations (4.10) and (4.11). This proportionality, is due to temporal coordinate time t and x, y, z as orthogonal spatial coordinates, where axis z is too temporal; t_1 and t_2 however, are in conjunction with superposition of charge e , or to be more specific,

$$\tau_\Sigma \propto \tau_0 \mid \text{if } x' = x = y, \Delta x' = \frac{\Delta x}{\sqrt{1 - v_{e,x}^2 c^{-2}}} \Rightarrow \lim_{y' \rightarrow x} (y' \neq y) \leftrightarrow \lim_{y' \rightarrow y} (y' = y)$$

$$\therefore z = r \mid f(r) \mapsto t,$$

where r , is the radial distance whose values are mapped to time coordinate t during angular change of r in (4.17) between trap sites with unity to Figs. 4.1 & 4.2. Hence, $\Delta\tau$ equals to

$$\sqrt{\Delta t^2 - \left(\frac{v_{e,x}\Delta t}{c}\right)^2 - \left(\frac{v_{e,y}\Delta t}{c}\right)^2 - \left\{ \left(\frac{v_{e,z}\Delta t}{c}\right)^2 \xrightarrow{\text{iff}} \left(\frac{\Delta t, \Delta t(x)_{xy}}{ct_x, t_y}\right)^2 + \left(\frac{\Delta ty_{xy} \vee y'_{xy}}{ct}\right)^2 \right\}}, \quad (4.12a)$$

where $\Delta t(x)_{xy}$ and Δty_{xy} or to the latter’s complement, $\Delta ty'_{xy}$, come from the two engaged fields, one time varying \mathbf{B} -field multiplied by its external field, and the other from CNT component across N and S poles of the staircase construction.

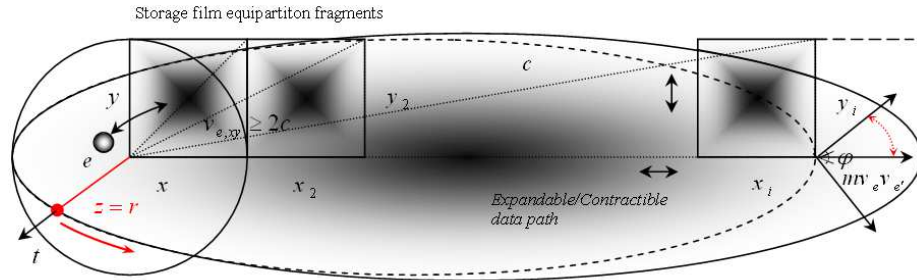


Figure 4.2. Charge storage film’s equipartition fragments or ‘trap sites’ of the memory cell enables the charge from the highly conductive localized CNT, to be stored. The induced charges in entanglement are also being stored once the quantized energy of the thin ONO film is associated with a nano-scale CNT channel. It is determined that this thin film has a quasi-quantized energy state due to the stored charges having a quantized voltage increment value as claimed by Choi *et al.* in [6]. This illustration also explains the paradoxical department of the storable data on an expandable data path meeting conditions of simultaneity on x_i, y_i of x', y' , solely when deductions of (4.12) are dealt with.

In continue, since if charge e , tends to travel both x and y directions simultaneously (here, being in two places at the same time), and thus sourced in favour of z (here, is

due to the travel from nano-thin layers of quantum wells or from lower electrode layers in an induced state to memory cell), charge e , should therefore possess a speed twice as much greater than its original speed relative to its speed performed in the memory cell's trap site. Consequently, after simplifying, we should then elicit,

$$\Delta\tau = \sqrt{\Delta t^2 - \left(\frac{v_{e,x}\Delta t}{c}\right)^2 - \left(\frac{v_{e,y}\Delta t}{c}\right)^2 - \left\{\left(\frac{v_{e,z}\Delta t}{c}\right)^2 \xrightarrow{\text{iff}} \left(\frac{\Delta tx}{ct_x}\right)^2 + \left(\frac{\Delta ty}{ct_y}\right)^2\right\}},$$

and when $\{x' = x = y\} \mapsto f(v_e)\Delta t$, thence,

$$\begin{aligned} & \therefore \sqrt{\Delta t^2 - \left(\frac{v_{e,x}\Delta t}{c}\right)^2 - \left(\frac{v_{e,y}\Delta t}{c}\right)^2 - \left\{2\left(\frac{\Delta tx}{ct_x}\right)^2\right\}} \\ & = \sqrt{\Delta t^2 - \left(\frac{v_{e,x}\Delta t}{c}\right)^2 - \left(\frac{v_{e,x}\Delta t}{c}\right)^2 - \left\{2\left(\frac{\Delta tx}{ct_x}\right)^2\right\}}, \\ & \therefore \Delta\tau = \Delta t \sqrt{1 - 2\left(\frac{v_{e,x}}{c}\right)^2 - 2\left(\frac{v_{e,x}|v_{e,xy} \geq c}{c}\right)^2} \leq \Delta t \sqrt{1 - \frac{4v_{e,x}^2}{c^2}} \end{aligned} \quad (4.12b)$$

where, $\tau_\Sigma \propto \tau_0 \left| \Delta\tau = \Delta t \sqrt{1 - 4\left(\frac{v_{e,x}}{c}\right)^2 - \left(\frac{v_{e,xy} \geq c}{c}\right)^2} \right.$, $x' = x = y$ and thus the following as,

$$\begin{aligned} \tau_\Sigma \propto \Delta\tau \left| \Delta\tau = \Delta t \sqrt{-4\left(\frac{v_{e,x}}{c}\right)^2 - \left(\frac{\sum_{i=2}^n i\right)^2} \right. & = \Delta t \sqrt{-\frac{4v_{e,x}^2}{c^2} - 4, \dots, n_{xy}^2} = \\ & 2\Delta t \sqrt{-9, \dots, n_{xy}^2 - \frac{v_{e,x}^2}{c^2}}. \end{aligned} \quad (4.12c)$$

For relative expanded geometric conditions where far memory cell's trap sites are of 'tuples or attribute square unit base by location', once $x' = x = y$ is established, for τ_Σ we then acquire,

$$\begin{aligned} \therefore \Delta\tau = \frac{2\Delta t}{c} \sqrt{-v_{e,x}^2 - 9, \dots, n^2 c_{xy}^2} & \leq \left\{ (t_1 | t_2) \cdot 2\Delta t \int_P dj = \frac{\Delta\tau}{2 \int_P dj} \cdot (t_2 | t_1) \right\} \lesssim (t_\Sigma^2 \\ & = \left(\frac{t_1+t_2}{\sqrt{2}}\right)^2), \end{aligned}$$

$$\therefore \tau_\Sigma^2 = \Delta t^2 \lim_{P \rightarrow -\infty} f(P) \xrightarrow{\Sigma} \int_P dj^{-1}, \text{ thus,} \quad (4.13)$$

$$\therefore \tau_\Sigma^2 = \frac{\Delta t^2}{2\Delta\tau (r \sum j)} = \frac{(t_1 | t_2) \dot{t}_0}{2(r \sum j)} = \frac{1(t_1 | t_2), 1(t_2 | t_1)}{dr \mapsto t}, \quad (4.14a)$$

$$\begin{aligned} \therefore \tau_\Sigma &= \frac{-\sqrt{t_1 |t_2 t_1|}}{\sqrt{2}\tau}, \frac{-\sqrt{t_2 |t_1 t_2|}}{\sqrt{2}\tau} = 1(t_1 |t_2), 1(t_2 |t_1) = \left\{ \begin{array}{l} |\dot{t}_0| \cos\left(\frac{\pi}{4}\right) \\ |\dot{t}_0| \sin\left(\frac{\pi}{4}\right) \end{array} \right\} \approx \\ 0.7071 |\dot{t}_0| &\equiv \tau_0, \end{aligned} \quad (4.14b)$$

or, equal to symmetric time in rest in the context of time depository in simultaneity. By definition,

$$\therefore \tau_\Sigma = \frac{\text{stationary time factor of past proper time data}}{\text{current proper time data} \times \text{radial time distance of complex plane integral}} \equiv \tau_0,$$

$$\varphi = \arg(z), \quad r = \sqrt{x^2 + y^2}, \quad x = r \cos \varphi, \quad y = r \sin \varphi \}. \quad (4.15)$$

An example of stored radar pulses is by time of events, t_E in (4.13), originated from Wright [41]'s discussions on relativity, now in favour of (4.15). Therefore, associating radial time distance r for a vector valued area of $d\mathbf{A}_{xy}$ which is perpendicular to electric displacement field \mathbf{D} , in terms of radial area dA_r , generates an electromotive force (emf), \mathcal{E} for (4.16), in a certain time interval divided by resistance R for the selective trap site area A . This selection of area occurs during field's displacement, since a time varying \mathbf{B} -field system on charge e for a closed loop capacitance is established, performing $e \xrightarrow{L_V, H_V} |\Psi\rangle$, as a free discrete structure of stored charges with respect to storable passing time τ , interdependent with time phase ϕ_2 , in regard to $WR.\phi_1 : RD.\phi_1$. This discrete structure urges to recall (1.6), §1, as an electromagnetic relation defining circuit's energy expectation. The behaviour derived from Maxwell's equations, is expressed as follows

$$\therefore \oint_C \mathbf{E} d\mathbf{I} \wedge A_r = \frac{-d\Phi_m}{dt} \nabla \cdot \mathbf{B} \cap A_r |\mathbf{D}| = \frac{dQA_r}{dA_{xy} \mapsto f_A} \equiv \frac{\mathcal{E}t}{RA}, \quad (4.16)$$

where \mathbf{E} , is the electric field, $d\mathbf{I}$, is the infinitesimal element of contour C . In the denominator, after implying $\nabla \cdot \mathbf{B} = A_r$, area A_{xy} is treated as a derivative of area function f_A , denoting the area with radial distance A_r promoted to some other 2D-trap site with index $x_i y_i$, otherwise remaining as xy for electric displacement field \mathbf{D} . Therefore, obtaining an asynchronous contour integral whilst in area-volume's geometric state of integration to the point of Ampere's Circuital law of capacitance extracted from Maxwell's 1861 paper [23]; and [27, viii], is thus plausible; or,

$$\therefore \int_A \oint \mathbf{D} d\mathbf{A}_{xy} dA_r = QA_{xy}^{-1} dA \mapsto A_{r \rightarrow x_i y_i} = QA_{xy}^{-1} A_{r \rightarrow x_i y_i}^{-1} J dr d\varphi = QA^{-2} r dr d\varphi, \quad (4.17)$$

$$\text{where, } J = \det \frac{\partial(x, y)}{\partial(r, \varphi)} = \begin{bmatrix} \frac{\partial x}{\partial r} & \frac{\partial x}{\partial \varphi} \\ \frac{\partial y}{\partial r} & \frac{\partial y}{\partial \varphi} \end{bmatrix} = r \cos^2 \varphi + r \sin^2 \varphi = r, \text{ explicitly,}$$

$$\begin{aligned} \therefore \frac{|\mathbf{D}|}{1 \leftrightarrow |\mathbf{A}_{yx}|} &= \left| \frac{QA}{2A^2} \right| \\ \leftrightarrow \int_V \rho_e(\mathbf{r}) dV &= \frac{Q_{free \rightarrow bailed \leftarrow free}}{2A_{freedom}} \equiv e \int |\psi(\mathbf{r})|^2 d\mathbf{r} = \frac{Q |\sqrt{QQ'}|}{2\sqrt{xy} A_{x_i y_i}} = \frac{Q}{2V}, \end{aligned} \quad (4.18)$$

where this therefore implies to $Q(t_2) \mapsto Q(t_2|t_1) \prec WR.\phi_1 : RD.\phi_1 \succ$ brought by subsequent relations, (4.19) and (4.20), and the $\therefore \frac{|D|}{1 \leftrightarrow |A_{yx}|}$'s right hand result in (4.18). The latter deduction in (4.18), is the charge density on the quantum capacitor's chosen plate via radial distance r between xy and $x_i y_i$, removing the problem of blocking flows of electric current due to the intrinsic nature of capacitors on charge's trap sites. Quantum charge density $\rho_e(\mathbf{r})$, in the same relation, represents continuous charge density of total quantum charge, $Q = e \int |\psi(\mathbf{r})|^2 dr$, over a volume \mathcal{V} , which could be either spherical or elliptical of the region (observe, Fig. 4.2). This regional volume conserving Q transformations, displays a readable displacing charge, $Q_{free \rightarrow new \text{ bailed on display}}$, converted into quantum charge density via wavefunction $\psi(\mathbf{r})$.

The momentum of the storable charge e as mv_e , also inflicts upon radial time change of (4.15), as De Broglie's wavelength representation of relativistic momentum, $p = \gamma m_0 v_e$ by Nave [25], convertible to a photon momentum, $h\lambda^{-1}$, as too, storable from light emitting conditions (e.g., ELEDs). The light emitting components, if used, are for representing photosensitive image-logic states, where mass in this case is stretched out with relevance to (1.4), §1, between all traps on charge e , as new $mv_e v_{e'} \in \prod E_e^{L_V \rightarrow H_V | \Psi}$, until the moment of charge deposit.

With relevance to the previous paragraph, the graph of the evolution of e 's mass is shown in Fig. 4.1 with the involved Gaussian curvature-states signifying the finite world of charge e , in the course of radial time. Tab. 4.1, also represents the evolution states of e 's mass in form of formulae. Generally, radial distance r , as radius of time t , is from the pole in the polar coordinate system converted from the Cartesian form on angle φ , defined on the complex plane. It is thus noted that the extraction and travel of charge e , in terms of $e^2 e_1 e_2$, is with restriction to time via \mathbf{B} -field lines (here as the carrier's worldline) of CCNT to the electric lines of transference, between xy and $x_i y_i$ via dA_r across the fields' flux volume.

In conjunction with (4.17), symbol ∇ , represents the del operator from the divergence theorem, where the $\nabla \cdot \mathbf{B} = 0$ representing no charge in the field's region, assumably tracks down radial distance wherever it ends up for charge e . This tracking of distance is defined as either condition of Σ in (4.9) between xy and $x_i y_i$ traps representing Σ^2 from (4.8), implied via compositional intersection $\nabla \cdot \mathbf{B} \cap A_r$ from (4.17). Also, destination area A in (4.16) and (4.17), is given as an area-element in the Cartesian coordinates, defined as an infinitesimal area relating to quantum dot before Cartesian conversion. Symbol J of (4.17), represents the Jacobean determinant of the coordinate conversion formula by (4.19) and (4.20). Charge e , is permitted to choose by freedom of choice via radial area A_r , where composition $A_{xy} A_r \rightarrow x_i y_i$ is stipulated according to the mapping, $dA \mapsto A_r \rightarrow x_i y_i$, of (4.17). This elementary area eventually expands into the memory cell's storage limit with reason to relations (4.17) and (4.16), ensuing (4.18) accordingly.

This is why semantically, choosing Q_{bailed} as a bailed quantity (provisionally $Q_{enclosed}$ in Gauss's law context) of electric charge e , becomes relevant to the data transmission operation. The total charge (Q) described as a 'bailed quantity', is a quantity of electric charge; a free charge provisionally remains free until the moment of trap. Let the opposing form be Q'_{bailed} , the chosen Q_{bailed} would then be expressed into a principle volume of charge conservation in terms of

$$\begin{aligned} Q(t_2) &= (t_1) + Q_{in} - Q_{out}, \text{ if } Q(t_2) \mapsto (t_2|t_1) \text{ thus, } \therefore Q(t_2|t_1) = \\ &Q(t_1|t_2) + Q_{in} - Q_{out}, \\ t_1 \underline{\succeq} WR.\phi_1 &\longrightarrow Q_{bailed} : RD.\phi_1 \longrightarrow Q'_{bailed} \underline{\preceq} t_2, \end{aligned} \quad (4.19)$$

$$\begin{aligned} \therefore t_2 \succ RD.\phi_1 &\longrightarrow Q'_{bailed} \equiv RD.\phi_1 \longrightarrow Q_{free \leftarrow bailed \rightarrow free} \equiv RD.\phi_1 \longrightarrow \\ Q_{free \rightarrow new\ bailed\ on\ display} & \end{aligned} \quad (4.20)$$

Discrete mathematical symbols, ‘precedes from’, \prec , and ‘succeeds from’, \succ , as time predecessors of write and read time phase ϕ_1 on charge density $Q(t_2)$ and $Q(t_2|t_1)$, are derived from (4.19) implied to Q_{bailed} and Q'_{bailed} respectively, which is well-defined in data read/write operations. The first part of (4.19), denotes the principle of charge conservation [27, v]; the second part however, as mapped, denotes the symmetric problem of a quantity of the elementary charge e , flowing into as Q_{in} and flowing out of the volume as Q_{out} between entangled time $(t_1|t_2)$ and $(t_2|t_1)$, simultaneously. The $(t_1|t_2)$ component in (4.19) and other conceiving relations from the past are ‘highly symmetric’, where the symmetry itself appreciates Noether’s Theorem explained by Baez in [1]; and [27, vi]. Reasoning that in this case for the time symmetry, the time variable is said to be at any locus to its increment/decrement position, thus entangled between at least 5 dimensions over a one-dimensional manifold (time) out of an N-dimensional universe. Hence $(t_1|t_2)$ or its symmetry $(t_2|t_1)$, ‘commutatively’ in logic, represents stationary time factor t_0 -dependant whilst being of proper time τ -dependant, as the stored past or future proper time τ_0 . Therefore, this duality of time in behaviour, advocates the reality of time factor \dot{t} , paradoxically in form of $\dot{t}^2 \neq \dot{t}^2$ from past relations (4.5) and (4.14b) pertinent to statements on the subject of Russell’s Paradox (e.g., [31]; [34]). This ‘time at rest symmetry’ is in the dilated magnetic moment μ of charge e , read and write time phase ϕ_1 , via evaluating ϕ_2 ’s feedback for the stored data-bit process (for more details, refer to §5). Bear in mind, this $(t_1|t_2)$ and its symmetry $(t_2|t_1)$ concept, is of

Theorem 4.1. *Let time barrier or restriction $(t_1|t_2)$, and its symmetry stand never an anomaly, since this method of representing time, is itself merely a ‘presentation of time continuity equation’ as a whole, which is constantly interconnected or intact to its past, current and future dilation. In satisfaction of this theorem, the following conditions would rely as equivalent:*

- (1) *The interconnectivity of time dilation, is independent to event occurrences whilst being dependent symmetrically to its proper (as proper time τ) and its rest, simultaneously.*
- (2) *The ‘rest time’ given in condition (1) of this theorem, could be of t_1 or t_1t_2 , as connecting past-to-future and the latter definition’s symmetry t_2t_1 , connecting future-to-past, correspondingly.*

Relations (4.12) to (4.20), do benefit from the basics of Einstein’s twin paradox in SR. Relevantly, say for instance, we imagine charge e as ‘stationary twin’ relative to its ‘travelling twin’ $e_2e'_2$ in Minkowski’s diagram [33]. Now for the e ’s travelling twin, envisage it to be confined into ‘plane of simultaneity’ via one space-time coordinate representing the occurred superposition, converting superposition data-length x_Δ^2 , into timelike scenario from the stored data’s past events. The past events indicate a space-like scenario for charge e due to ‘minimum velocity favouring a dimensional-course of entanglement’ in quantum scales of quantity, or,

$$\begin{aligned} \forall x_\Delta^2 \in \sum^2 |x_\Delta \equiv \\ \frac{f(x_{\Delta 0})}{\lim_{\tau_\Sigma \rightarrow \infty} v \circ |\tau_\Sigma|} &= \frac{v_e t_{(x_i y_i, x y) \leftrightarrow z}}{t_{z \leftrightarrow (x y, x_i y_i)} \sqrt{\frac{-4v_e^2 - c^2}{v_e^2 |c^2}}_{z \leftrightarrow (x y, x_i y_i)}} = \frac{v_e^2 t_1 t_2}{2\tau |v_{e, z \leftrightarrow (x y, x_i y_i)}| \sim c} \end{aligned}$$

$$= x_{\Delta} \mathbf{o} \sum^2, \text{ where,}$$

$$c_{z \leftrightarrow (xy, x_i y_i)} \stackrel{\hat{=}}{=} v_{e, z \leftrightarrow (xy, x_i y_i)} \stackrel{\hat{=}}{=} v_e, \lambda = \frac{x_{\Delta 0} x_{\Delta}}{x_{(xy, x_i y_i)}} = n \cdot p = \frac{p^2}{2\Delta p}, n \in \mathbb{R}^{3 \rightarrow 2n} \quad (4.21)$$

satisfying conditions of $v > c$ from foundations of SR, expectably (e.g., [2]). These conditions occur solely, once the velocity factor is taken out of radical expression in the denominator shown in (4.21).

This relation appreciates Einstein's modified first law i.e. 'no matter can travel faster than the speed of light' wherein this case, charge e is not travelling faster than c , in fact, the entangled coordinate systems' implication via axis ratio $z \leftrightarrow (xy, x_i y_i) : (x_i y_i, xy) \leftrightarrow z$, folds time itself giving out a spacelike problem indeed! Compare this relation with image logic on Moiré pattern as an interferometric approach [27] which describes the limits of pale and dark zones of pattern for the superimposed lines.

Furthermore, imagine two misaligned patterns geometrically possess a $x_{\Delta 0} \times x_{\Delta}$ non-relativistic-relativistic distance or x_{Δ}^2 , from the point of hot electron emission per complete pattern distance $x_{(xy, x_i y_i)}$, where electrons are bombarded on screen upon either pattern p of Δp , in coordinates time $t_{(xy, x_i y_i) \leftrightarrow z}$. It is thus conceivable that travelling back and forth to either generated carriers' path (the modulus usage is for this reason only), forming aligned or even the same pattern's initial result, should thereby obtain wavelength λ -result in (4.21). The resultant of this pattern could be mapped into the characteristics of the ONO film representing quantized energy states of the storage system and employed to develop optoelectronic property.

Notation $\mathbb{R}^{3 \rightarrow 2n}$ in (4.21), represents the subspace notion of Darboux's Theorem commencing with a Euclidian space geometry to a range of '2n-dimensional vector space configuration' upon the involved carriers' parametric properties such as, pattern recognition, travelled distance(s) and their entangled loci as well.

Accordingly, the symbolic choice of ' $\hat{=}$ ' by definition 'stands for. . .', is by Dickinson & Goodwin of [12] on issues of schema calculus in discrete mathematics. Hence, for one the discrete property of (4.21) conceives and therefore propagates logic upon the outputs no matter the constraints of this expectation. The discrete mathematical concept on these logic outputs, shall institute the condition of true realistic outcome frame representing the only plausible resultant as a 'cavity system' and some 'display system' conducting all the factual states of reality between 'Boolean logic and image-logic states'. Ergo,

Hypothesis 4.2. *'Image logic' is in manifestation as an optical course of absorption-spontaneous emission versus stimulated emission cycle manifestation, once the remaining classical binary and quantum factors of memory cells serve charge e , with wavelength λ , proper to its pattern state given in Eq. (4.21). The following proof by deduction, leads to the current hypothesis:*

Proof by deduction. *This pattern state of Eq.(4.21) emerges an image of the charge's confinement, the uncertainty at the point of superposition and thus, a depository vector point of closure confining now past, current and future of that same charge in xy cellular dimensions, or its neighbouring $x_i y_i$ cellular dimensions. Selective mass ratio of charge e , in \mathbf{B} -field for its periodic energy pattern via Tab.4.1, is measured with the Zeeman effect. This effect is analogous to the photon type of e 's excited atomic state such as an optical course of absorption-spontaneous emission versus stimulated emission cycle.*

5 Memory cell's time and data representation, chip's compatibility and comlink

The following shall bring about the very basics in expert analysis on time-data signaling issues and events of computational logic in emerging forms of quantum logic and classical binary logic or 'Boolean logic'; whereas the anticipated logic would embed into its structure the electrical states and the time-data bits of information. This anticipation of logic is contemplated in the well-known terminology used for databases, data structures and algorithms such as, 'data atoms' and their property of how data is being transformed from one stage of compilation to another.

For this type of time-data versus data-time analysis process, the following Subsections basically give a glimpse of time-data in its representation frame in a simplified manner, especially, for those hypothetical conditions previously submitted in §4. That is, explaining the role of Gaussian curvature in Minkowski's space and time universe into transformable Euclidean and non-Euclidean planes of geometry. This kind of geometric transformation is illustrated and discussed in §§5.2. The following Subsection, commences with the electrical states as classical and quantum logic, forming the main part of time-data against data-time constituents.

5.1 Time-data input's classical and quantum logic states

Based upon Fig. 2.1d, §2, design and logic, by changing the sheet resistance, R_s value, for source and drain electrodes in either pole of the memory system, the p.d. circuitry distribution thereby generates a compatible technology to other FET transistors (or, FET family). Most appropriately, DCFL logic would be compatible in board's layout, subsequent to the chip's fabrication process in some simulating 'circuit maker' environment. Potency of data input against data output in this circuit requires registers incorporated into the circuit's logical representation of its computational data, hence to evaluate time phase ϕ_1 and ϕ_2 values for $WR.\phi_1$ and $RD.\phi_1$. Subsequently, it would be possible to verify the evaluation process on refreshing time cycles via ϕ_2 's feedback for the stored data-bit with respect to the stored qubits from the *waterfall effect* components i.e. CCNTs' memory cells, in practice. The cyclic problem in storing data could be complied within form of, bit ratio \mathfrak{R}_{bit} , representing data of any type per time function $f(t)$, as being refreshed periodically for a time and space-varying data (compare this with 'a semi-static RAM cell design and logic' from Pucknell & Eshraghian of [30]). In this case, time function $f(t)$, represents time t -of- ϕ_2 or, in abstract algebraic terms of mapping and mappability $t \circ \phi_2$, devoted to ratio bit \mathfrak{R}_{bit} , and bit frequency ν_{bit} , where the latter is measured in Hertz accordingly. In other words,

$$\begin{aligned} \nu_{bit} &\equiv \frac{\mathfrak{R}_{bit}}{t} = \frac{in_{bit}}{in_{qbit} \times f(t)} = \frac{\forall A \in \{0, 1\}}{\forall B \in \{(\partial \cdot B + \bar{\partial} \cdot B), \Delta B (\tilde{\partial} \cdot B)\} \times t \circ \phi_2} \\ &= \frac{\{0, 1\}}{\{(0\ 1), (1\ 0), (1\ 1), (0\ 0)\} \times t}, \end{aligned} \quad (5.1)$$

and by methods of simplification,

$$\therefore \nu_{bit} \equiv \frac{A_{in}}{B_{in}t} \left| \text{for } A_{in} \left\{ \begin{array}{l} 0 \triangleq L_{\pm V} \\ 1 \triangleq H_{\pm V} \end{array} \right\} \text{ for } B_{in} : |\Psi\rangle = \prod_{m=1}^n |\Psi\rangle_m, m = 1, 2, \dots, n, \text{ thus,} \right.$$

$$(0\ 1) \equiv \left(\lim_{\forall e \in 0V \rightarrow 0} 0.0\dots \times e, \lim_{\forall e \in V_S \rightarrow \infty} e \right) \in (L_{\pm V} H_{\pm V}) , \quad (5.2)$$

$$\therefore (0\ 1) \equiv \left(\sum 0.0\dots \times e, \sum e \right) = (0V\ V_S) : |\psi\rangle = a|0\rangle + b|1\rangle, \quad (5.3)$$

$$\text{where } a \text{ and } b \text{ are complex numbers such that, } 1 = \sqrt{|a|^2 + |b|^2}. \quad (5.4)$$

Wavefunction $|\psi\rangle$ representing pure qubit states could extend, once the recording by n -qubit quantum register, the state of B_{in} registers between the chip's subsystems establishes, which therefore requires 2^n complex numbers, accordingly (e.g. Ref. [11]).

In relation (5.3), V_S is the high level logic and $0V$, is the low level logic, whereas both states appreciate differential signaling, here as the ends of the same logic defining one qubit of information in quantum computing for signal B_{in} ; supposedly, the superposition of all the classically allowed logic states like A_{in} now being for B_{in} in wavefunction $|\psi\rangle$, to be as follows:

————— Let index notation $\pm V$, in either (5.2) or (5.3), represent a typical applied signal in favour of high and low logic states. By obvious reasons, $\pm V$ would specify whether the conventional current I , for the potential difference occurrence is of either direction to the opposite flow direction of electrons multiplied by resistance R , derivable from Ohm's law $I = VR^{-1}$. It is then with resemblance to (5.3), in ratio to $|\psi\rangle$, for the remaining state outcomes on signal B_{in} , states $(1\ 0)$, $(0\ 0)$ and $(1\ 1)$ as $(V_S\ 0V) : |\psi\rangle$, $(0V\ 0V) : |\psi\rangle$ and $(V_S\ V_S) : |\psi\rangle$ achieved respectively, which are thereby predicatively conventional. —————

Bear in mind, low level logic does not necessarily mean the p.d. occurrence to be purely 0 volts, and it was the delimitation factor that formulated the present scenario representing the 'quantum tunneling problem' in clarity between all charges for input signal B_{in} . An example of quantum tunneling, classically-forbidden energy state, is given in relation (1.4), §1, recalling events of $\prod E_{e\ L_V, H_V|\Psi}$ for Σ of relation (4.11), §4, on charge e . Charge e in this case, is with restriction to being entangled with e_2 as e_1e_2 , otherwise, entangled with e_2 's symmetry as e_2e_2' . Time t_1 , however, is with restriction to t_2t_1 as $\dots t_1|t_2t_1$ in ratio to proper time τ , for depository's space two-dimensional restriction xy to x_2y_2 as $(xy|x_2y_2)\tau$.

This notion of space-time entanglement for charge e in terms of, $(xy|x_2y_2)\tau$, could also represent the cell's neighbouring storage frame, whereas for the involved logic signals of (5.1) and (5.2), are expressed in terms of total charge Q from relations (4.18-4.20) of §4, or,

$$\forall B_{in}, A_{in} \in H_S \left| \int_{\mathcal{V} \rightarrow H_S} \rho_e(\mathbf{r}) d\mathcal{V} = \frac{Q}{2\mathcal{V}} \right., \text{ whereby, from (5.3) then,} \quad (5.5)$$

$$\therefore (A_{in}, B_{in}) \equiv (Q, Q|\sqrt{QQ'}) : |\psi\rangle, \text{ and,} \quad (5.6)$$

$$\therefore \prod E_{e\ L_V, H_V|\Psi} \xrightarrow{|\Psi\rangle} \left\{ \forall B_{in} \in H_S \overset{\mathbb{R}_{bit}(in_{bit})^{-1}}{\rightarrow} in_{qbit} \times f(t) \right\}, \text{ such that,} \quad (5.7)$$

$$(\partial \cdot B, \bar{\partial} \cdot B) = (\nabla B + \Delta B, \bar{\nabla} B + \bar{\Delta} B), \text{ and,}$$

$$\bar{\partial} \cdot B = \nabla B + \bar{\nabla} B + \bar{\Delta} B \text{ in (5.1) for, } \int_S \phi_2 d\phi_2. \quad (5.8)$$

Let with recall to (5.1) and (5.2), input A_{in} in (5.5) and (5.6), represent a logic signal of 0 or 1. For relations (5.5) to (5.9), input B_{in} , represents a combinatorial quantum signal from EDL events' logic occurrence introduced by Talantsev of [36]; where symbol $\bar{\partial}$, represents 'no change' or 'non-event' in quantum signal; ∂ , represents any change in the same quantum signal, B , accordingly (see also [30], §11). It is noteworthy to mention that, event-driven logic (EDL) prior to the direct coupled FET logic (DCFL) inverters' integration for the bus line at time t , is contemplated as the most suitable in describing qubit storage behaviour. This form of inverters' integration represent the change of logic from 0 to 1 and vice versa. The integration also includes the no-change conditions on 0 or 1 logic, explaining whatever the logic is in-between high and low logic states as variant logic, suspended in the *waterfall effect* storage system's scenario.

Bear in mind, the product sequence $0.0\dots \times e$ in (5.2), would denote that no electron or most conditionally, a few electrons satisfy a 'low state logic'. On the one hand, these electrons represent the x coordinate of some testing electronics graph for input signal B_{in} 's two dimensional coordinate system of $(x y)$ on p.d. 'high and low state logic' occurrences. On the other hand, other logical conditions would imply to the remaining coordinates B_{in} against the well-known Boolean logic on signal A_{in} , as by propositional restrictions established in (5.2).

In continue, assuming for minimum ν_{bit} in either pole α or β , as $\min \nu_{bit}$, and for the expected ν_{bit} in both poles α and β , as $\nu_{bit} \big|_{\beta}^{\alpha}$, we then obtain respectively,

$$\min \nu_{bit} = \frac{1\text{bit}}{2\text{bit}_{|\Psi\rangle} \times 10^{-n}\text{s}} = 0.5 \times 10^n \text{ Hz},$$

$$\nu_{bit} \big|_{\beta}^{\alpha} = \sum_{\substack{m \geq i \\ l \geq j \\ i=1 \\ j=2}} \frac{i\text{bit}}{2j\text{bit}_{|\Psi\rangle} \times 10^{-n}\text{s}} \geq 0.5 \times 10^n \text{ Hz}. \quad (5.9)$$

Components $2\text{bit}_{|\Psi\rangle}$ and $2j\text{bit}_{|\Psi\rangle}$ in the denominator of ν_{bit} and $\nu_{bit} \big|_{\beta}^{\alpha}$ in (5.9), represent 1q-bit and $1jq$ -bit, respectively, where index, $|\Psi\rangle$, denotes any entangled Bell state for binary storable value, 'bit' of information. By means of which, $2\text{bit}_{|\Psi\rangle}$ or $2j\text{bit}_{|\Psi\rangle}$ for signal B_{in} , is defined in some Hilbert space $H_{\mathbf{S}}$ of (5.5) to (5.9), for any involved system satisfying $|\Psi\rangle$ in terms of one-dimensional to N-dimensional expandability; discussed via relations (1.1 to 1.9), Theorem 1.1, and Proof 1.1, §1. Notation \mathbf{S} in $H_{\mathbf{S}}$, represents the signal subsystem as a state of quantum system, in this case, the storable B_{in} signal. The Hilbert's subsystem time-domain integral on time phase ϕ_2 , satisfies the storable signal B_{in} in (5.8) by the system's EDL characteristics, whilst classical signal A_{in} is being stored via bit-frequency ν_{bit} of (5.9).

In the context of SR, Hilbert space $H_{\mathbf{S}}$'s patterns on quasi-particle as dual carriers in discrete subspaces on carrier e 's space would basically derive Tab. 4.1, §1. The space given to quantum charge as e 's space, is described to be a superspace constructed by fields from §4. Tab. 4.1's consequent equations, resemble with dual superboson (superfermion) characteristics based on quasi-particle algebras, relations (3.3) to (3.5), §3, by Temme in [37], with the definition of supersymmetric systems, by Popowicz in [29], respectively.

5.2 Comlink time-data representation

The comlink in terms of telecommunication link between two devices, requires the least understanding of data transmission for all data sender and receivers installed onto the communications network system. It is thereby studied that, the importance of why one should embrace the nature of science in terms of timing and data transmission where all communications between biological systems (e.g., humans) and artificial systems (e.g. satellites and their dishes), establish plausible contacts between them in space and beyond. This includes planet Earth, when the concept of relative information is being investigated concurrently. Therefore, realizing the following comlink time-data diagram and algorithm (or, comlink TDDA) example as a theoretical system, helps scientists to cope with asynchronous situations on data transmission between receivers and senders in terms of time-data synchronization, preventing time/data delay event occurrence(s). The hardware connection behaving as instantaneous conversion of asynchronous into synchronous situations would be of a PTVD-SHAM protocol, which defines the behaviour in its image logic buffering state (see Ref. [27, xii]).

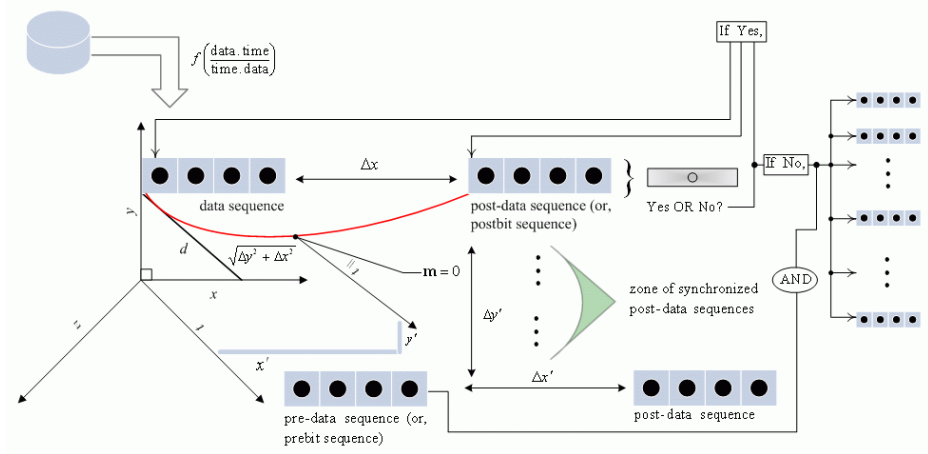


Figure 5.1. A comlink TDDA example allows a practical engineer to investigate the theoretical concept of data-time versus time-data for all progressing computations thoroughly in terms of data function in relation (1a), §1, as updated in the present figure.

Nevertheless, bringing closer the collected data from a destination object (or body e.g., a non-stellar body like our moon), to source (assuming the source to be a sender/receiver unit), is the main objective yet to be accomplished (see Fig 2.2, §§2.2). The result of this close capture or scope displacement of the frequency in transmission, would be data frequency enhancement on the frequency's configuration and resolution (for imagery and photo-analysis purpose). This includes the receiptment of solar images in shorter lengths of time compared to the usual course of recordings due to the nature of Gaussian curvature scenarios explicated in Tab. 4.1, §4, on charge, e .

Consider the following geometric predicate explaining events of both Figs. 5.1 and 5.2. All of these events are to be related to planar and coordinate transformations in Euclidian space geometry when all concerning events are described by the time aspect as well. The time aspect deforms the geometry to a geometry that stores events of time-data/data-time, conditionally. The deformed geometry can be written in the

form of

$$\left\{ \forall (P P') \in \widehat{PP'} \left| \begin{array}{l} \widehat{PP'} = [\{\mathbf{m}\} \cap \{d\}] \cup [\{\mathbf{m}'\} \cap \{d'\}] = \left[\left\{ \frac{\Delta y}{\Delta x} \right\} \cap \right. \\ \left. \left\{ \sqrt{\Delta y^2 + \Delta x^2} \right\} \right] \cup \left[\left\{ \frac{\Delta y'}{\Delta x'} \right\} \cap \left\{ \sqrt{\Delta y'^2 + \Delta x'^2} \right\} \right] \\ (P P') = (\{\mathbf{m}_i\} \cap \{d_i\} \quad \{\mathbf{m}'_i\} \cap \{d'_i\}) , \quad i \in \mathbb{N} \end{array} \right. , \left. \right\} \quad (5.10a)$$

$$\text{where, } \mathbf{m} = \frac{\Delta y}{\Delta x} = \frac{y_2 - y_1}{x_2 - x_1}, \quad (x_2 \neq x_1). \quad (5.10b)$$

This is a geometric predicate, and (5.10a) explicates the position of data sequence illustrated in Fig. 5.1, in terms of two-dimensional variables such as xy and xz , in a coordinate transformation for that involved data. This data type could be of post-data sequence otherwise, pre-data sequence in form of time, measured in seconds and data, measured in bits. The steepness (or gradient) and direction is measured by slope \mathbf{m} , as specified in (5.10b), which points out the range of involvements in two dimensional displacements of plane H to H_i for the two-dimensional variables mentioned recently, where index $i \in \mathbb{N}$.

The geometric plane-to-plane shifting from $H_{xy} \rightarrow H_i$ to H_{xz} between quadrants $(+, -)$ and $(+, +)$ for plane H_{xy} , and $(-, +)$ for plane H_{xz} , during Cartesian coordinate transformation of data sequence to post-bit sequence, is in accordance with the given algorithm in Fig. 5.1. The planar shift could also be expressed in terms of multiple integral or in this case, an *extended triple definite integral*. This integral type for a volume \mathcal{V} of time-data revolution with restriction to data-time in state of, 'data \odot time \odot data' from (1a), §1, could be computed where time t is being involved between all planar states of geometry in respect to its parallel. That is in cases of, data $\odot \odot t_{\parallel}$, and, data $\odot \odot t_{\parallel}$, satisfying product $\mathcal{V}t$, as in form of t -standard and t_{\parallel} -central, respectively, (5.14). The time involvement mentioned, ensues by chance, a space-time fold as noted in Fig. 5.2 (pay attention to the erected arrow from C'); that is,

firstly, we assume the following geometry using propositional operators in the foundations of logic, for the shifting planes of H within quadrants $(+, -)$ and $(+, +)$:

whilst possessing by assumption, $\overline{AC} \parallel \overline{A'C'}$, $\overline{CB} \parallel \overline{C'B'}$, we also manage to write

$$\widehat{AB} \cap \widehat{B'A'} = \left\{ \widehat{AB} - (\widehat{AP'} + \widehat{PB}) \right\} \cup \left\{ \widehat{B'A'} - (\widehat{B'P'} + \widehat{PA'}) \right\} = \widehat{PP'}, \quad H_{xy} \parallel H_i \quad (5.11)$$

then, applying plane(s) function \mathfrak{P} , to shapes and curves of Fig. 5.2, comes *second* in definition, whereby

$$\begin{aligned} \mathfrak{P}(\widehat{ABC} \cap) &\equiv \mathfrak{P}(\widehat{ABC} - \widehat{ACBA'C'B'}) = \mathfrak{P}(\widehat{ABC}) \cap \mathfrak{P}(\widehat{B'A'C'}) = \\ (\forall H_{xy} \in (+, -) \cap H_i) \cup (\forall H_{xy} \in (+, +) \cap H_i) &= \mathbf{A} \approx \sum_{i=1}^m \sum_{j=1}^n f(P_i, P'_j) A_{ij} \end{aligned} \quad (5.12)$$

ergo, deducing the concerning 'integral type' mentioned in the previous paragraph is obtainable in form of

$$\mathcal{V}_{\text{data} \odot \text{time} \odot \text{data}} = \int \int \int_{\mathcal{R}} f(x y x' y') d\mathbf{A} dt = \int \int \int_{\mathcal{R}} f(y x t) dx dy dt, \quad (5.13)$$

wherein the obtained multi-integral system, defines the morphism of variables, x' and y' , in their continuous function form, whilst they lie on the parallel real line (or parallel real axis) into time variable, t , it is thereby written

$$\{\forall t \in \mathcal{V}t \mid t^2 \rightarrow tt_{\parallel} \rightarrow t \wedge t \rightarrow tt_{\parallel} \rightarrow t^2 :: \text{true}\} , \therefore t \leftrightarrow t_{\parallel} \leftrightarrow t^2 , t \rightarrow \log_t (tt_{\parallel}) = 2 \quad (5.14)$$

where \mathcal{R} in (5.13), is the region of integration in the Cartesian plane \mathbb{R}^2 or simply, the integration in the xy -plane and xz -plane, as known in their geometric representation (see Fig. 5.2), H_{xy} and H_{xz} (or, H_{xz} 's complement symmetry, H'_{xz} -plane), respectively. This kind of integration, results once again $\mathbb{R}^{3 \rightarrow 2^n}$ for a subspace system studying vector events in Euclidian geometry elicited from Darboux's Theorem (revisit relation 4.21, §4). Note that H'_{xz} plane, is equivalent to H_{zx} for each spotted time-data or data-time unit according to unit representation in (1a), §1. Furthermore, the physical concept of H_{zx} prior to its geometric representation, is akin to the notion preformed in Fig. 5 of [54] which too, satisfies real-time events in gathering critical/essential information to the database system.

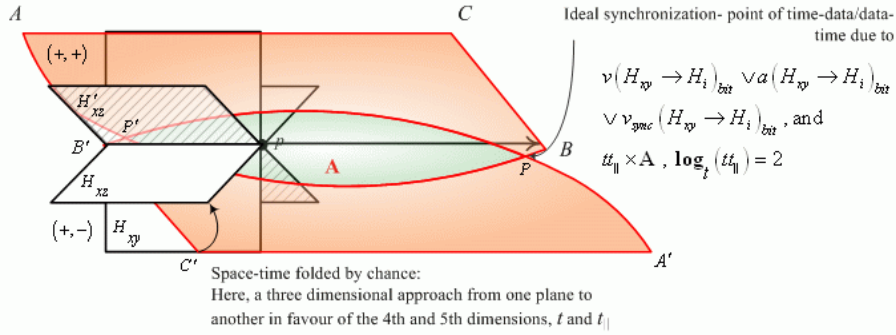


Figure 5.2. A time-data/data-time system with an infinite number of solutions for its geometry, relevant to Fig. 5.1.

Therefore, the problem of time synchronization between space-time dimensions, due to the planar revolution concurrence between isometric Euclidean planes of H to H_i subsequently produces a non-Euclidean isometry [27, xx]. It is at that point, conducting data from source to destination in the PTVD-SHAM system is tenably attainable, just as illustrated in Fig. 5.2. The transformation of Cartesian type in Fig. 5.1 could be mapped to the geometry illustrated in Fig. 5.2, whilst taking into consideration the Gaussian elimination mentioned in [53], for the infinite solution. An 'infinite solution' is expressed in terms of sorting the problem of the integrating area \mathbf{A} and thus, time synchronization between space-time dimensions, conducting data from source to destination in the PTVD-SHAM system.

This system representing infinite number of solutions is *consistent* and is in accordance with Theorem 2.1 on p. 43 of [53]. These geometric relationships between planes of H , results into velocity of the involved plane, where a probable planar acceleration a , is consequential to a synchronized frame of the same velocity between its initial state to its accelerative state. That is, the synchronized velocity v_{sync} , as the most privileged state of all sets of planar velocities regarding planes of H , or,

$$v(H_{xy} \rightarrow H_i)_{bit} = \frac{\vec{pB}}{t} , a(H_{xy} \rightarrow H_i)_{bit} = \frac{\vec{pB}}{tt_{\parallel}} , v_{sync}(H_{xy} \rightarrow H_i)_{bit} = \frac{\vec{PP'}}{t} \quad (5.15)$$

where time t , is involved between all planar states of geometry in respect to its parallel t_{\parallel} , as indicated in probable planar acceleration a , considering both time frames in one, is measured in meter squared. These time parameters corroborate with the chance of space-time fold in virtue of logarithm $t \rightarrow \log_t (tt_{\parallel}) = 2$, which persists upon a cyclical split of time into two time frames, t and t_{\parallel} or *time* powered by 2 in the logarithmic relation. Furthermore, planar velocities are being probabilistically/cyclically transformed due to, $t^2 \rightarrow tt_{\parallel} \rightarrow t \wedge t \rightarrow tt_{\parallel} \rightarrow t^2$ and its equivalence $t \leftrightarrow t_{\parallel} \leftrightarrow t^2$, as if time and its parallel is being cyclically dilated under time-data/data-time functional circumstances. Instances of Minkowskian space-time supersymmetric system [29], are now simplified into the Euclidian and non-Euclidean vector events, e.g., the geometric scalar transformations \vec{pB} and \vec{PB} , justly represent the travelled distance for time-data between coordinates dedicated to planar transformation concurrence, $H_{xy} \rightarrow H_i$, in terms of

$$v(H_{xy} \rightarrow H_i)_{bit} t, a(H_{xy} \rightarrow H_i)_{bit} t^2 \text{ for } \vec{pB} \text{ and, } v_{sync}(H_{xy} \rightarrow H_i)_{bit} t \text{ for } \vec{PB}. \quad (5.16)$$

The above-mentioned ‘time-data/data-time functional circumstances’, would maintain a global positioning system for any unit that installs and initiates PTVD-SHAM, satisfying ‘velocity and gravitational time dilation combined-effect tests’ [27, xvi]. This would allow operating experiments in both special and general relativity, e.g., accurate time-dilation effects as best average points for the effects’ rate on clocks across the surface of Earth and satellite systems such as the ones given in Figs. 2.2, 2.3 of §2.

6 Conclusion and future remarks

The empirical rudimentary concept of data output on the functions of SHAM’s architecture from §3, shall be submitted in the future reports. In those progressing reports, e.g., transmission electron microscopy (TEM imaging) on the chip’s components such as CCNTs relevant to the findings of Biró *et al.* [3]; Pack *et al.* [28], is concluded once the testability features of the entire components are gathered upon. Unambiguously, in those reports, as exemplified in, §§3.2, the data collection would be comprised of: a set of phases of data analysis, error reporting procedure and experimentation prior to design objectives and logic. The analysis and presentation stage of data will be based on the experimental methods of [17] and simulation kits, e.g., ‘Fast Henry inductance analysis tool’ proposed by Pack *et al.* of [28], 2D and 3D physics-based simulation e.g., ATLAS device simulator [47].

Treatment of storing data by complex plane’s depository vector system defining storable qubit(s), permits one to signify the importance of integrating components that detect quantum property of particles in a controlled manner; for instance, briefly, the current paper introduces ‘Catalysts, Cavity’s Quantum Property via CNTs, Memory Cells and CCNTs as CNFETs’ in its body map.

The next pace to take is aimed for structured facts once the researcher develops a report on the SHAM chip project. The objective would be a significant step to store data without worrying about the timing process, data’s best location in addressing and thereby, on software programming issues, one not being concerned about levels of program coding and compilation(s).

The other implications of this design is accomplishing devices as timepiece and clocks, winding time by themselves, e.g., picking up electromagnetic pulses for radar

systems from any satellite and non-satellite application (e.g., planetary phenomena) source, for any communications' wavelength in different geographical locations including our solar system and beyond. The reason would be the physical approach of highly oscillated bits of information acting sufficient in channeling through the blocks of electrical circuit, and then efficiently located and put into secondary memory locations for data-read and write, correspondingly. These premises of the application have been introduced in form of basic diagrams and the drawn conclusions from propositions, in §§2.2, §§2.3, hence their work mechanism on time-data throughout §5, respectively.

No matter the classical constraints involved in electronics' design and principle, once the grip of this technology holds its grounds by incorporating the *waterfall effect*, circuitry, narrowing down and simplifying data analysers, program processors on the chip, is deemed to be achievable exponentially. For instance, whilst possessing a magnitude of ∞ , asymptotically, for the orientation of array displacement as the present issue is organized with, even considering HDD defragmentation process on data would not be necessary based on PTVD-SHAM's technological aspects. There are those algorithms that endure to test results on the chip's compatibility and characteristics specifying, *frequency narrowbanding of infinite bands of incoming information from the chip's surrounding environment and beyond*.

In conclusion, once this technology is utilized in terms of CCNTs and CNFETs, data computation beyond quantum computational speed is deemed to be achievable. This so-called 'breaking the computational speed limit', can happen, if the geometry of the fabrication process is finalized as a freedom of point on circuit's layout, conductivity and responsivity, revealing the expected vales from hidden variables of the experiment.

Statement of conclusion:

——— *Assume in the laws of quantum physics that, any assigned value as an input is pondered to bring about the notion of 'uncertainty'. On the contrary, conjecturing the notion of certain reserved locations for data by pre-defined time in entanglement (predetermined on anticipated time) for uncertain values, is itself upon any individual which tends to read/write data and time, understood as a 'certainty'!* ———

The Author

Acknowledgements

The work described in this paper was supported personally as an extension to the basis of a scientific book, research project license no: TXU001347562, USA (1998-2007), and an extension to, arXiv: 0707.1151 Ref. [57], from the same author. The author thanks, Gerald Goodwin & Martin Dickinson of the Faculty of Technology, Department of Computing, University of Lincoln, UK (2005), for their departmental written confirmation on behalf of the author's personalized scientific activities.

References

- [1] J. Baez (Mathematical Physicist), 'Noether's theorem in a nutshell' (2002), see for instance, <http://math.ucr.edu/home/baez/noether.html>, accessed on 14. May 2007
- [2] B. Bassett and R. Edney, *Introducing Relativity*, 'Einstein's modified first law...' pp. 59,73, 2002.

- [3] L. P. Biró *et al.*, ‘Scanning tunneling microscopy of tightly wound, single-wall coiled carbon nanotubes’, *Europhys. Lett.*, Vol. **50** (4), pp. 494–500, 2000.
- [4] S. Bose, V. Vedral and P. L. Knight, ‘A Multi-particle Generalization of Entanglement Swapping’, the entanglement swapping scheme of Zukowki *et al.*, *Quant. Phys. ArXiv.org.*, pp. 1-4, 2006.
- [5] Y. F. Chen, Y. T. Dai and I. Lo, ‘Abstract, Observation of double cyclotron resonance in modulation- δ -doped In_{0.52}Al_{0.48}As/In_{0.53}Ga_{0.47}As heterostructure by optical detection’, *App. Phys. Lett.*, *Amer. Inst. Phys.*, Vol. **68** (8) pp. 1117-1119, 1996 (doi:10.1063/1.115731)
- [6] W. Choi, I. Yoo and J. Chu, Memory Device Utilizing Carbon Nanotubes, Samsung Co., Ltd. U.S. patent no. US 7015500 (2006).
- [7] A. Clark, A. Karch, P. Kovtun and D. Yamada, ‘Tensionless strings and free scalar fields’, *session H4-Particle Phys.* University of Washington, *Amer. Phys. Soc.* 2004.
- [8] C. L. Cohen *et al.*, ‘Metallic Carbon Materials’, US patent no. 5,993,697 and; hybrid nanotube on <http://www.lbl.gov/Tech-Transfer/techs/lbnl1180.html> (1998).
- [9] P. G. Collins and P. Avouris, ‘Nanotubes for Electronics’, *Sci. Amer. J.* , p. 68, 2000.
- [10] P. Delaney and J. C. Greer, Classical computation with quantum systems, *Proc. R. Soc. A Vol. 462*, 117–135, 2005.
- [11] D. P. Di Vincenzo, ‘Quantum Computation’. *J. Sci. Vol. 270* (5234): 255-261. Retrieved on 2007-04-25, 1995.
- [12] M. Dickinson (Ph.D.) and G. Goodwin, ‘Mathematics I & II Lecture Notes on *Discrete Mathematics*’, University of Lincoln, UK. (2002-2005).
- [13] A. Einstein, ‘Zur Elektrodynamik bewegter Körper’, *Annalen der Physik*, Vol. **17**, 891 (1905). English translation: On the electrodynamics of moving bodies.
- [14] A. Einstein, H. A. Lorentz, H. Weyl, and Minkowski, *The principle of relativity* pp. 83-91, 1952.
- [15] D. R. Greenberg, J. J. Pekarik and J. Scholvin, ‘Multilevel interconnection for an integrated circuit chip’, patent no. 2006/0289994 A1 (2006).
- [16] H. J. Kim, Y. W. Jin, Han I. T. & H. W. Lee, Method of Vertically Aligning Carbon Nanotubes Using Electrophoresis, US patent no. 2006/0131172 A1 (2006)
- [17] L. Kirkup, *Experimental Methods: an introduction to the analysis and presentation of data*, Australia: John Wiley and Sons Press, 1994.
- [18] C. Kittel *Introduction to Solid State Physics*. John Wiley & Sons, Inc., pp. 784-778, 1996.
- [19] M. Krämer and B. Jacobs *et al.* ‘Strongly Reduced Gate Lag in Undoped AlGa_N/Ga_N HEMTs on Sapphire’ pp. 618-621 (2003).
- [20] S. G. Krantz, ‘the term point at infinity is also used for complex infinity’ p. 82, or see for instance, <http://functions.wolfram.com/Constants/ComplexInfinity/19/04/> (1999).
- [21] P. Lambin, G. I. Mark and L. P. Biro, ‘Structural and electronic properties of coiled and curled carbon nanotubes having a large number of pentagon–heptagon pairs, abstract’, sect. 3 & 6-electronic properties & conclusions, respectively, *Phys. Rev. B*, Vol. **67**, 205413, 2003.
- [22] D. R. Leadley, Reduced Dimensional Structures, Warwick University, (1997), see for instance: <http://www.warwick.ac.uk/~phsbm/2deg.htm>, accessed on 02. June 2007.
- [23] J. C. Maxwell, ‘On physical lines of force’, Ampère’s Circuital law at equation (112), *J. Sci.* 1861.
- [24] J. H. McGuire and A. L. Godunov, ‘Quantum Time Entanglement of Electrons’, *Amer. Phys. Soc.*, see for instance, <http://adsabs.harvard.edu/abs/2002APS..APR.X4004M> (2002).

- [25] C. R. Nave, *Hyper Physics*, ‘Relativity’, *Dept. of Phys. and Astrophys.* Georgia State University, 2005.
- [26] H. Okita , K. Kaifu *et al.* ‘High transconductance AlGa_N/Ga_N-HEMT with recessed gate on sapphire substrate’, 2003 ([doi:10.1002/pssa.200303537](https://doi.org/10.1002/pssa.200303537))
- [27] *Online encyclopedia* (2007) **i-** Qubit, entanglement see, for instance: [Qubit](#); **ii-** Complex plane see, for instance: [Complex plane](#); **iii-** Maxwell’s continuity equation, see, for instance: [Maxwell’s equations in curved spacetime](#); **iv-** 2DEG description, see, [2DEG](#); **v-** Charge conservation, mathematical representation of its law, see, [Charge conservation](#); **vi-** Noether’s theorem, Noether’s current, see, [Noether’s theorem](#); **vii-** Discrete mathematics, functions and relations, see, [Functions and relations](#); **viii-** Corrected Ampère’s Circuital law: the Ampère-Maxwell equation; see, [Ampère’s Circuital law](#); **ix-** Line moiré, superposition of layers, see, [Line moiré](#), also see, Moiré of parallel patterns, interferometric approach, [Line moiré](#); **x-** Effective mass see, for instance: [Effective mass](#); **xi-** Faraday effect and atomic line filter, see, [Atomic line filter](#); **xii-** Optical buffer, see for instance: [Optical buffer](#); **xiii-** Terminal element, see for instance: [Terminal element](#); **xiv-** Cost estimation models, see for instance: [Cost estimation model](#); **xv-** Proper time in special relativity, see for instance: [Proper time](#); **xvi-** Time dilation, see for instance: [Time dilation](#); **xvii-** Logic programming, see for instance: [Problem solving](#) or, Algorithm, visit: [Problem solving](#); **xviii-** General quantum interference, see for instance: [Interference](#); **xix-** Iterative method, see for instance: [Iterative method](#); **xx-** Euclidean plane isometry, see for instance: [Euclidean plane isometry](#); **xxi-** Protocol, see for instance: [Protocol \(computing\)](#); **xxii-** Big \mathcal{O} notation, see for instance: [Big \$\mathcal{O}\$ notation](#); **xxiii-** Quantum logic, see: [Quantum logic](#); **xxiv-** Linearization, see: [Linearization](#); **xxv-** Geometric progression, see: [Geometric progression weblink](#).
- [28] M. Pack *et al.*, ‘Novel designs for nano-scale inductors’. *Calif. Inst. Tech.* pp.1-5, 2004.
- [29] Z. Popowicz, ‘Integrable System Constructed out of Two Interacting Superconformal Fields’. *Inst. Theor. Phys. University of Wroclaw, Poland, Quant. Phys. ArXiv.org.*, pp. 7-8, 1997.
- [30] D. A. Pucknell and K. Eshraghian, *Basic VLSI Design* (3rd Ed.) Prentice-Hall Silicon Systems Engineering, chaps. 4, 9 & 11, sect. 4-2, 4-2-1; 9-1, 9-2-1-2, 9-2-3, 9-2-3-4; 11-6-1, 11-6-1-1, 11-6-1-2, 11-6-1-3, 1994.
- [31] W. Quine, ‘On the theory of types’, *J. of Symbolic Logic* 3. ‘Incidentally, this theorem and the definition of collection it builds on, are Potter’s first theorem and definition, respectively’, 1938.
- [32] Z. F. Ren *et al.* , *J. Sci.* **282**, 1105, 1998.
- [33] W. Rindler, *Relativity: Special, General and Cosmological*. Oxford University Press (2001), ISBN 0-19-850836-0.
- [34] B. Russell, *Principles of Mathematics*. Cambridge: Cambridge University Press, chap. X, sect. 100, 1903.
- [35] G. Saathoff *et al.* ‘Relativistic Doppler effect in the theory of special relativity’, *Presentation of the Guido Saathoff modern reenactment of the Ives-Stilwell experiment, Max-Planck-Inst.*, 2007.
- [36] A. D. Talantsev, ‘on the analysis and synthesis of certain electrical circuits by means of special logical operators’, *Autom. and Telemekh.* **20**, 895-907, 1959.
- [37] F. P. Temme, ‘On quasi-particles algebra’, *Proc. R. Soc. A Vol.* **461**, 328-329, 2005.
- [38] Texas Instruments, *High-performance linear products technical staff*, LVDS Application and Data Book, 2002, lecture no. SLLD009
- [39] Y. Umeno, T. Kitamura and A. Kushima, ‘Metallic–semiconducting transition of single-walled carbon nanotubes under high axial strain’, *Dept. of Eng. Phys. and Mech., Kyoto University, Japan, Elsevier B.V.*, 2004 ([doi:10.1016/j.commat.2004.01.033](https://doi.org/10.1016/j.commat.2004.01.033))
- [40] X. Wang, Y. Liu and D. Zhu, ‘Pillar-shaped structures and patterns of three-dimensional carbon nanotube alignments’, *R. Soc. Chem. Commun.*, pp.751-752, 2001 ([doi:10.1039/b100326g](https://doi.org/10.1039/b100326g))

- [41] E. L. Wright (Ph.D.), ‘Time dilation; radar’ on: Relativity Tutorial webpage. *Astro. Phys.*, UCLA, 2006.
- [42] P. Hariharan, ‘Simple, high-efficiency, single-photon trap detectors’ *J. Opt. B: Quantum Semiclass. Opt.* **1** 522-523, 1999 (doi:10.1088/1464-4266/1/5/304)
- [43] A. Joshi and P. Rheingans, ‘Illustration-inspired techniques for visualizing time-varying data’ on <http://www.cs.umbc.edu/~alark1/illustration.pdf>, University of Maryland Baltimore County, *Proceedings of IEEE Visualization*, pp. 679-686, 2005.
- [44] J. Hedin, Design and Construction of a Potassium Faraday Filter for Potassium Lidar System Daytime Operation at Arecibo Observatory, LULEÅ UNIVERSITY LIBRARY [link accessed on March 25, 2006] p.16, 2002.
- [45] Kapany and Burke entitled ‘Optical Waveguides’; Academic Press. N.Y. and London, 1972, pp. 233-257.
- [46] J. M. Senior, *Optical fiber communications*, (2nd Ed.), Prentice Hall International (UK), Ltd., chap. 7, 1992.
- [47] SIMUCAD and SILVACO, ‘process and device, 2D and 3D physics-based simulation’ <http://www.silvaco.com/company/corpBrochure300dpi.pdf> , accessed on 02. June 2007.
- [48] Kodak Co. , ‘Charge-couple device (CCD) image sensors’, image sensor solutions Rochester, NY, USA, on <http://www.kodak.com/ezpres/business/ccd/global/plugins/acrobat/en/supportdocs/chargeCoupledDevice.pdf>, (2001).
- [49] S. Knappe, V. Gerginov *et al.*, ‘Atomic vapor cells for chip-scale atomic clocks with improved long-term frequency stability’, *Opt. Lett.*, Vol. **30**, Issue 18, pp. 2351-2353, 2005.
- [50] J. C. Howell *et al.*, ‘All-optical delay of images using slow light’, *Phys. Rev. Lett.*, Vol. **98**, 043902, 2007.
- [51] Robert Kowalski, ‘Algorithm=Logic+Control’, *Communications of the ACM* **22** (7): 424-436, 1979 (doi:10.1145/359131.359136)
- [52] F. H. Musa, MOSFET comparator, Ltd. U.S. patent no. **US 3956708**, (1976).
- [53] S. Lipschutz and J. J. Schiller, *Finite Mathematics* (2nd Ed.), ‘linear equations and their graphs’ and ‘systems of linear equations’, chaps. 1 & 2, pp.3-43, 1995.
- [54] Kai Zeng, Erwei Bai and GeWang, A Fast CT Reconstruction Scheme for a GeneralMulti-Core PC, *Int. J. Biomed. Image., Amer. Inst. Phys.*, (29160) pp. 1-9, 2007 (doi:10.1155/2007/29160)
- [55] Nikos Drakos, Time-frequency Resolution, *Stanford Exploration Project* on <http://sepwww.stanford.edu>, 1997.
- [56] David M. W. Powers. Parallelized Quicksort with Optimal Speedup. Proceedings of International Conference on Parallel Computing Technologies. Novosibirsk. 1991.
- [57] P. B. Alipour, ‘Logic, Design and Organization of Prallel Time Varying Data and Time Super-helical Memory As; PTVD-SHAM’, article id. arXiv: 0707.1151, *CompSci. Ar. ArXiv.org.*, pp. 1-33, 2007.